# Numerical experiments with the Bloch–Floquet approach in homogenization

## C. Conca[1], S. Natesan[2] and M. Vanninathan[3, *, †]

[1]*Departamento de Ingeniería Matemática, Facultad de Ciencias Físicas y Matemáticas,*
*Universidad de Chile, and Centro de Modelamiento Matemático, UMI 2807 CNRS-UChile,*
*Casilla 170/3—Correo 3, Santiago, Chile*
[2]*Department of Mathematics, Indian Institute of Technology, Guwahati, 781 039, India*
[3]*TIFR Center, IISc Campus, P.O. Box 1234, Bangalore 560012, India*

## SUMMARY

This paper deals with a numerical study of classical homogenization of elliptic linear operators with periodic oscillating coefficients (period $\varepsilon Y$). The importance of such problems in engineering applications is quite well-known. A method introduced by Conca and Vanninathan [*SIAM J. Appl. Math.* 1997; **57**:1639–1659] based on Bloch waves that homogenize this kind of operators is used for the numerical approximation of their solution $u^\varepsilon$. The novelty of their approach consists of using the spectral decomposition of the operator on $\mathbb{R}^N$ to obtain a new approximation of $u^\varepsilon$—the so-called Bloch approximation $\theta^\varepsilon$—which provides an alternative to the classical two-scale expansion $u^\varepsilon(x) = u^*(x) + \Sigma \varepsilon^k u_k(x, x/\varepsilon)$, and therefore, $\theta^\varepsilon$ contains implicitly at least the homogenized solution $u^*$ and the first- and second-order corrector terms.

The Bloch approximation $\theta^\varepsilon$ is obtained by computing, for every value of the Bloch variable $\eta$ in the reciprocal cell $Y'$ (Brillouin zone), the components of $u^*$ on the first Bloch mode associated with the periodic structure of the medium. Though theoretical basis of the method already exists, there is no evidence of its numerical performance. The main goal of this paper is to report on some numerical experiments including a comparative study between both the classical and Bloch approaches. The important conclusion emerging from the numerical results states that $\theta^\varepsilon$ is closer to $u^\varepsilon$, i.e. is a better approximation of $u^\varepsilon$ than the first- and second-order corrector terms, specifically in the case of high-contrast materials.

KEY WORDS: homogenization; periodic structures; Bloch waves; numerical solution of differential equations; finite element method

*Correspondence to: M. Vanninathan, TIFR Center, IISc Campus, P.O. Box 1234, Bangalore 560012, India.
†E-mail: vanni@math.tifrbng.re.in

## 1. INTRODUCTION

Multi-scale problems in science and engineering are often described by partial differential equations (PDEs) with highly oscillating coefficients. Typical examples include composite materials with fine micro-structures and highly heterogenous porous media. The direct numerical simulation of problems involving multi-scale solutions is difficult due to the requirement of tremendous amount of computer memory and CPU time which can easily exceed the limit of today's computer resources. On the other hand, in practice, it is often sufficient to compute with certain accuracy approximate solutions incorporating large-scale features of the original solution. Thus, various methods of *up-scaling* or *homogenization* have been developed which replace the governing equations with multi-scale solutions by a simple set of equations for the homogenized (or effective) solutions which can be resolved on a coarse scale mesh. For more applications of homogenization theory in Physics, Engineering and Mechanics one may refer to References [1–3].

For a nice introduction to this subject, the reader is referred to the book of Bensoussan *et al.* [4]. The main result states that the (weak) limit of solutions in domains with periodic micro-structures resolves a suitable boundary-value problem with constant coefficients that represent what is known as homogenized medium. There are many ways to obtain the homogenized coefficients and there is a vast body of work in the literature which justifies the limiting process. In Reference [4], the authors used the method of two-scale expansion to homogenization and their technique is the most traditional way to obtain the homogenized medium. Further, they introduced the concept of correctors of various orders to capture (interior) oscillations of the solution.

Conca and Vanninathan [5] gave a new proof of convergence using Bloch wave decomposition. Further, they offered a non-traditional way of calculating the homogenized coefficients and more precisely, they proved that the classical homogenized matrix coincides with one-half of the Hessian of the first Bloch eigenvalue $\lambda_1(\eta)$ at the origin. In a more recent paper [6], they introduced what they called the *Bloch approximation* function $\theta^\varepsilon$ to the solution $u^\varepsilon$ of the original problem. This function provides a sharp approximation in the sense that it contains implicitly, in some sense the homogenized solution and the classical correctors of all orders which were first obtained by Bensoussan *et al.* [4] by using a two-scale asymptotic expansion for the solution. It is rigorously established that in the case of smooth coefficients, $\theta^\varepsilon$ contains the first- and second-order correctors (see Theorem 1.11 in Reference [6]). As mentioned above, the theoretical basis of the Bloch approximation is provided in Reference [6]. However, its numerical performance is lacking in the literature.

Our principal goal in this paper is to provide some numerical experiments concerning Bloch approach to the homogenization process. Further, a comparative study between the classical and Bloch approaches in one- and two-dimensional cases is also carried out.

In order to implement Bloch waves numerically one has to obtain an accurate approximation of a parameterized family of spectral problems in a representative cell, say $Y = ]0, 2\pi[^N$ with a generalized periodic condition. The main difficulty here is to treat these generalized periodic conditions numerically. This is done by using the idea of projection which includes an exponential complex weighted average between the values on opposite faces. After discretization, each of these spectral problems reduce to a generalized eigenvalue problem of the Sylvester's type which can be solved numerically by standard algorithms. In order to find the homogenized coefficients, a fourth-order finite difference formula is used to obtain the Hessian of the first

Bloch eigenvalue at $\eta = 0$. This involves the computation of $\lambda_1(\eta)$ in a small *ad hoc* grid around the origin.

To determine the so-called Bloch approximation function $\theta^\varepsilon$, we have to calculate the first Bloch eigenvector and then apply a quadrature formula to approximate the integral numerically. The important conclusion from the numerical results states that in the case of smooth coefficients, $\theta^\varepsilon$ provides better approximation to $u^\varepsilon$ than the classical first- and second-order corrector terms. This is due to the fact that the first Bloch mode $\phi_1(\cdot; \eta)$ is an analytic function of the Bloch variable $\eta$ (for small $\eta$) and one can therefore expand it in a Taylor series around the origin. Thus it contains lot of information and in particular, it is proved that the first- and second-order corrector terms are included in $\theta^\varepsilon$ in the case of smooth coefficients. If we expand up to the first-order term, we obtain an approximation $\tilde{\theta}^\varepsilon$ which in its turn is an approximation of $u^\varepsilon$, too. The numerical calculation of $\tilde{\theta}^\varepsilon$ is slightly simpler than the one of $\theta^\varepsilon$ and the numerical experiments reported in Section 5 show that its performance is more similar to the first-order corrector term. All these facts are extensively illustrated in Section 5 of this paper by several examples in both one- and two-dimensional cases.

Apart from being a theoretical tool in homogenization problems, the Bloch approximation $\theta^\varepsilon$ is an interesting object for practical reasons too. Whether the coefficients are smooth or not, it is always in the energy space $H^1(\mathbb{R}^N)$ in which lies the original solution $u^\varepsilon$, which enables us to compare them both. In contrast, the classical correctors of Reference [4] do not enjoy this property in general unless severe regularity hypotheses are made ($u^* \in H^2(\mathbb{R}^N)$, $\chi_k \in W_\#^{1,\infty}(Y)$, etc.). Under such regularity hypotheses, it is shown in Reference [6] that $\theta^\varepsilon$ contains first- and second-order correctors introduced in Reference [4]. It is therefore clear that $\theta^\varepsilon$ is an object of interest incorporating multi-scale features of the original solution even in non-regular cases. Our computations in one- and two-dimensional cases demonstrate that the Bloch approximation is superior to second-order corrector in terms of accuracy, especially in the case of certain high-contrast materials; while Bloch approximation performs well, classical correctors exhibit spurious oscillations. Further, comparing CPU times for the classical correctors and $\theta^\varepsilon$, we note that the CPU time for $\theta^\varepsilon$ is greatly reduced when $\varepsilon$ is small. Our numerical experiments reveal this phenomena. However, it is as such incapable of describing boundary layer oscillations present in the solution; classical correctors too suffer the same fate. To capture the boundary oscillations, we must study the interaction of Bloch waves with the boundary which is a topic for the future. Some efforts have been taken in this direction by Allaire and Conca [7] in the case of spectral problems.

Though it is yet to be carried out, it is clear to us that Bloch approach could be extended to a medium where the coefficients are not periodic but only locally periodic. The main difference between the two cases is as follows. It is possible to eliminate $u^*$ in the expression for $\theta^\varepsilon$ in the periodic case, whereas it is not possible in the locally periodic case. In the later case, we must solve the homogenized equation for $u^*$ at the mesh points, then use an appropriate algorithm like fast Fourier transform to determine $\widehat{u^*}$. Then, via a suitable quadrature rule we can compute $\theta^\varepsilon$ from (16).

There are various multi-scale methods available in the literature. We would like to mention some of them. Avellaneda *et al.* [8] and Orive *et al.* [9] used finite difference method to solve this type of problems, whereas Hou *et al.* [10] applied multi-scale finite element method. Further, we would like to mention a recent work [11], in which the Bloch–Floquet approach is used to provide new homogenization results and handles the boundary layer terms for frequency-dependent problems. Finally, it must be said that every method has its own domain

of validity and limitations. In the work [10], suitable finite element bases are introduced to capture local oscillations in the solution. Compared to these methods, ours is a spectral approach in which we exploit the first Bloch mode associated with the periodic structure to suggest an approximation for these oscillations. It is generally known that spectral methods are more expensive but more accurate compared to physical space methods, see References [12, 13]. This partly explains why Bloch approximation is superior to the classical correctors.

Before proceeding further, we mention a word about the notations adopted in the sequel. Unless mentioned explicitly, the usual summation convention with respect to the repeated indices is understood. The constants appearing in various estimates independent of $\varepsilon$ are generically denoted by $c$. Apart form the usual norms in Sobolev spaces $H^1$, we will also use the following semi-norm:

$$|v|_{H^1} = \left\{ \sum_{j=1}^{N} \|D_j v\|_{L^2}^2 \right\}^{1/2}$$

The rest of the paper is organized as follows. Classical homogenization results are presented in Section 2. Section 3 deals with the Bloch waves. The computational aspects of the Bloch waves are given in Section 4. Section 5 presents numerical results supporting the method.

## 2. CLASSICAL HOMOGENIZATION RESULTS

In this section, we shall present the classical homogenization results which include the homogenized operator, the first- and second-order correctors.

Consider the operator

$$A \overset{\text{def}}{=} -\frac{\partial}{\partial y_k} \left( a_{k\ell}(y) \frac{\partial}{\partial y_\ell} \right), \quad y \in \mathbb{R}^N \tag{1}$$

where the coefficients satisfy

$a_{k\ell} \in L_\#^\infty(Y)$ where $Y = ]0, 2\pi[^N$, i.e. each $a_{k\ell}$ is a

$Y$-periodic bounded measurable function defined on $\mathbb{R}^N$, and $\tag{2}$

$\exists \alpha > 0$ such that $a_{k\ell}(y)\eta_k\eta_\ell \geqslant \alpha|\eta|^2 \quad \forall \eta \in \mathbb{R}^N, \ y \in Y$ a.e.

$a_{k\ell} = a_{\ell k} \quad \forall k, \ell = 1, \ldots, N$

We also consider a zeroth-order term with coefficient $c \in L_\#^\infty(Y)$, $c(y) \geqslant 0$.

For each $\varepsilon > 0$, we also consider the operator $A^\varepsilon$ where

$$A^\varepsilon \overset{\text{def}}{=} -\frac{\partial}{\partial x_k} \left( a_{k\ell}^\varepsilon(x) \frac{\partial}{\partial x_\ell} \right) \quad \text{with } a_{k\ell}^\varepsilon(x) = a_{k\ell}\left(\frac{x}{\varepsilon}\right), \quad x \in \mathbb{R}^N \tag{3}$$

In homogenization theory, it is usual to refer to $x$ and $y$ the slow and the fast variables, respectively. They are related by $y = x/\varepsilon$. Associated with $A^\varepsilon$, let us consider the following

boundary-value problem

$$A^\varepsilon w^\varepsilon + c\left(\frac{x}{\varepsilon}\right) w^\varepsilon = g \quad \text{in } \Omega, \quad w^\varepsilon \in H_0^1(\Omega) \tag{4}$$

which is posed in an arbitrary bounded domain $\Omega$ in $\mathbb{R}^N$ and $g$ is a given element in $L^2(\Omega)$. The boundary of $\Omega$ is denoted by $\Gamma$. It is classical that the above problem admits one and only one solution. Our aim in this paper is to describe numerically the interior oscillations of the solution as $\varepsilon \to 0$. This problem is equivalent (see Reference [6]) to the consideration of a sequence $u^\varepsilon$ in $H^1(\mathbb{R}^N)$ and a function $f$ in $L^2(\mathbb{R}^N)$ satisfying

$$A^\varepsilon u^\varepsilon + c\left(\frac{x}{\varepsilon}\right) u^\varepsilon = f \quad \text{in } \mathbb{R}^N$$

$$u^\varepsilon \rightharpoonup u^* \quad \text{in } H^1(\mathbb{R}^N)\text{-weak} \tag{5}$$

$$u^\varepsilon \to u^* \quad \text{in } L^2(\mathbb{R}^N)\text{-strong}$$

In the sequel, we will describe the oscillations of $u^\varepsilon$ via the Bloch approximation. While applying this result to the problem (4) it is natural to take $u^*$ to be the homogenized solution of (4) extended by zero outside $\Omega$ and $f$ to be equal to $g$ extended by zero outside $\Omega$. This is perfectly justified since we are interested in the approximation of $w^\varepsilon$ in relatively compact open subsets $\omega \subset\subset \Omega$. It is true that the localization process gives rise to lower-order terms in the equation. This can be treated as in Reference [14].

To describe the oscillation of $u^\varepsilon$, it is natural to introduce a *first-order corrector*, namely a function $u_1^\varepsilon$ in $H^1(\mathbb{R}^N)$ which should be easily constructed, and have the following characteristic property:

$$\|u^\varepsilon - u^* - \varepsilon u_1^\varepsilon\|_{H^1(\mathbb{R}^N)} \to 0 \quad \text{as } \varepsilon \to 0 \tag{6}$$

In the same spirit, a *second-order corrector* $u_2^\varepsilon \in H^1(\mathbb{R}^N)$ will enjoy the property

$$\|u^\varepsilon - u^* - \varepsilon u_1^\varepsilon - \varepsilon^2 u_2^\varepsilon\|_{H^1(\mathbb{R}^N)} \leqslant c\varepsilon \tag{7}$$

Bensoussan *et al.* [4] obtained an asymptotic expansion for the solution of (5) in the following form:

$$u^\varepsilon(x) = u^*(x) + \varepsilon\chi_k(y)\frac{\partial u^*}{\partial x_k}(x) + \varepsilon^2 \chi_{k\ell}(y)\frac{\partial^2 u^*}{\partial x_k x_\ell}(x) + \cdots \tag{8}$$

Here, $\chi_k$ is the unique solution of the cell problem

$$A\chi_k = \frac{\partial a_{k\ell}}{\partial y_\ell} \quad \text{in } \mathbb{R}^N$$

$$\chi_k \in H_\#^1(Y), \quad \mathcal{M}_Y(\chi_k) \stackrel{\text{def}}{=} \frac{1}{|Y|}\int_Y \chi_k \, dy = 0 \tag{9}$$

where $H^1_\#(Y)$ is the space of $H^1$-functions which are $Y$-periodic, and it will be defined in the next section. The function $\chi_{k\ell}$ is characterized as the unique solution of

$$A\chi_{k\ell} = a_{k\ell} + a_{km}\frac{\partial \chi_\ell}{\partial y_m} - \frac{\partial}{\partial y_m}(a_{mk}\chi_\ell) - \mathscr{M}_Y(a_{k\ell}) - \mathscr{M}_Y\left(a_{km}\frac{\partial \chi_\ell}{\partial y_m}\right) \quad \text{in } \mathbb{R}^N$$

$$\chi_{k\ell} \in H^1_\#(Y), \quad \mathscr{M}_Y(\chi_{k\ell}) = 0$$

(10)

The first term in (8) satisfies the homogenized equation

$$A^*u^* + c^*u^* \overset{\text{def}}{=} -q_{k\ell}\frac{\partial^2 u^*}{\partial x_k \partial x_\ell} + c^*u^* = f \quad \text{in } \mathbb{R}^N$$

$$u^* \in H^1(\mathbb{R}^N)$$

(11)

where the homogenized coefficients are given by

$$q_{k\ell} = \mathscr{M}_Y\left(a_{k\ell} + a_{km}\frac{\partial \chi_\ell}{\partial y_m}\right) \quad \forall k, \ell = 1, \ldots, N$$

$$c^* = \mathscr{M}_Y(c)$$

(12)

(If we work on $\Omega$, then the boundary condition $u^* = 0$ on $\Gamma$ will be imposed on $u^*$.) The zeroth-order term $c(x/\varepsilon)u^\varepsilon$ does not contribute to the definition of Bloch waves to be introduced in the next section. Its only contribution is the zeroth-order term $c^*$ in the homogenized equation (11).

Above asymptotic expansion (8) suggests naturally the following choices for the correctors:

$$u_1^\varepsilon(x) = \chi_k(y)\frac{\partial u^*}{\partial x_k}(x)$$

and

$$u_2^\varepsilon(x) = -\chi_{k\ell}(y)\frac{\partial^2 u^*}{\partial x_k x_\ell}(x), \quad y = \frac{x}{\varepsilon}$$

However, it must be pointed out that the above elements are not in $H^1(\mathbb{R}^N)$ unless the solutions of the cell problem $\chi_k$, $\chi_{k\ell}$ and the homogenized solution $u^*$ are sufficiently smooth. In stark contrast, the *Bloch approximation* introduced below will be always in $H^1(\mathbb{R}^N)$. This is a virtue of the approximation suggested in this paper.

## 3. BLOCH EIGENVALUES AND EIGENVECTORS

Here, in this section, we will outline the theoretical background of Bloch waves which is going to be implemented numerically in the next section.

Conca and Vanninathan [5] gave an alternative formula for the homogenized coefficients defined in (12). They have studied the spectral resolution of $A$ in $L^2(\mathbb{R}^N)$. For this, they have used the classical method of Bloch [15] which consists of introducing a family of spectral

problems parametrized by $\eta \in \mathbb{R}^N$: find $\lambda = \lambda(\eta) \in \mathbb{R}$ and $\psi = \psi(y; \eta)$ (not identically zero) such that

$$A\psi(\cdot; \eta) = \lambda(\eta)\psi(\cdot; \eta) \quad \text{in } \mathbb{R}^N, \quad \psi(\cdot; \eta) \text{ is } (\eta; Y)\text{-periodic, i.e.}$$
$$\psi(y + 2\pi m; \eta) = \mathrm{e}^{2\pi i m \cdot \eta}\psi(y; \eta) \quad \forall m \in \mathbb{Z}^N, \ y \in \mathbb{R}^N \tag{13}$$

By using the transformation

$$\psi(y; \eta) = \mathrm{e}^{i\eta \cdot y}\phi(y; \eta), \quad \phi(\cdot; \eta) \text{ is } Y\text{-periodic}$$

problem (13) becomes

$$A(\eta)\phi = \lambda\phi \quad \text{in } \mathbb{R}^N, \quad \phi \text{ is } Y\text{-periodic}$$

where the operator $A(\eta)$ is defined by

$$A(\eta) \stackrel{\text{def}}{=} -\left(\frac{\partial}{\partial y_k} + i\eta_k\right)\left(a_{k\ell}(y)\left(\frac{\partial}{\partial y_\ell} + i\eta_\ell\right)\right)$$

Here, the operator $A(\eta)$ is referred to as the shifted operator. It is clear from (13) that the $(\eta, Y)$ periodicity condition is unaltered if we replace $\eta$ by $(\eta + q)$ with $q \in \mathbb{Z}^N$ and $\eta$ can therefore be confined to the *dual cell* $\eta \in Y' = [-\frac{1}{2}, \frac{1}{2}[^N$ (Brillouin zone).

It is well-known that, due to ellipticity and symmetry hypothesis, the above problem admits a unique sequence of eigenvalues with the following properties:

$$0 \leqslant \lambda_1(\eta) \leqslant \cdots \leqslant \lambda_m(\eta) \leqslant \cdots \to \infty$$

$$\forall m \geqslant 1, \quad \lambda_m(\eta) \text{ is a Lipschitz function of } \eta \in Y'$$

Besides, the corresponding eigenfunctions denoted by $\psi_m(\cdot; \eta)$ and $\phi_m(\cdot; \eta)$ form orthonormal bases in the spaces of all $L^2_{\text{loc}}(\mathbb{R}^N)$-functions which are $(\eta; Y)$-periodic and $Y$-periodic respectively; these spaces are denoted by $L^2_\#(\eta; Y)$ and $L^2_\#(Y)$. It is worthwhile to remark that these eigenfunctions belong in fact to the spaces $H^1_\#(\eta; Y)$ and $H^1_\#(Y)$, respectively, where

$$H^1_\#(\eta; Y) = \left\{\psi \in L^2_\#(\eta; Y) \ \left|\ \frac{\partial \psi}{\partial y_k} \in L^2_\#(\eta; Y) \quad \forall k = 1, \ldots, N\right.\right\}$$

$$H^1_\#(Y) = \left\{\phi \in L^2_\#(Y) \ \left|\ \frac{\partial \phi}{\partial y_k} \in L^2_\#(Y) \quad \forall k = 1, \ldots, N\right.\right\}$$

In the literature $\{\lambda_m(\eta)\}_{m \geqslant 1}$ are referred to as Bloch eigenvalues and $\{\phi_m(\cdot; \eta)\}_{m \geqslant 1}$ as Bloch eigenvectors or Bloch waves.

The following theorem gives the relation between the above eigenvalue problem and the homogenized coefficients $q_{kl}$ and the $\chi_k$'s as defined in (12) and (9), respectively.

*Theorem 3.1* (*Conca and Vanninathan* [5])

We assume that $a_{k\ell}$ satisfy (2). Then there exists $\delta > 0$ such that the first eigenvalue $\lambda_1(\eta)$ is an analytic function on $B_\delta \overset{\text{def}}{=} \{\eta \mid |\eta| < \delta\}$, and there is a choice of the first eigenvector $\phi_1(y; \eta)$ satisfying

$$\eta \to \phi_1(\cdot; \eta) \in H^1_\#(Y) \text{ is analytic on } B_\delta$$

$$\phi_1(y; 0) = p^{(0)} \quad \left( = |Y|^{-1/2} = \frac{1}{(2\pi)^{N/2}} \right)$$

Moreover, we have the relations

$$\lambda_1(0) = 0, \quad D_k\lambda_1(0) \overset{\text{def}}{=} \frac{\partial\lambda_1}{\partial\eta_k}(0) = 0 \quad \forall k = 1, \dots, N$$

Further, the Hessian of $\lambda_1$ at $\eta = 0$ is given by

$$\frac{1}{2}D^2_{k\ell}\lambda_1(0) \overset{\text{def}}{=} \frac{1}{2}\frac{\partial^2\lambda_1}{\partial\eta_k\partial\eta_\ell}(0) = q_{k\ell} \quad \forall k, \ell = 1, \dots, N \tag{14}$$

The derivatives of the first Bloch mode can also be calculated and they are as follows:

$$\frac{\partial\phi_1}{\partial\eta_k}(y; 0) = \mathrm{i}|Y|^{-1/2}\chi_k(y) \quad \forall k = 1, \dots, N \tag{15}$$

Let us consider the sequence $u^\varepsilon$ satisfying hypotheses (5). The Bloch approximation of $u^\varepsilon$ is defined by the following formula:

$$\theta^\varepsilon(x) \overset{\text{def}}{=} \frac{1}{\varepsilon^N} \int_{Y'} \widehat{u^*}\left(\frac{\eta}{\varepsilon}\right) \mathrm{e}^{\mathrm{i}(x/\varepsilon)\eta}\phi_1\left(\frac{x}{\varepsilon}; \eta\right) \mathrm{d}\eta, \quad x \in \mathbb{R}^N \tag{16}$$

where $\widehat{u^*}$ is the classical Fourier transform of the homogenized solution $u^*$, and $\phi_1$ is the first Bloch mode.

We conclude this section with the following two theorems of Reference [6] which provide an estimate for the difference between $\theta^\varepsilon$, $u^\varepsilon$ and the classical first- and second-order corrector terms.

*Theorem 3.2*

Assume that the coefficients $a_{k\ell}$ satisfy (2). Let $u^\varepsilon$ be the sequence introduced in (5). Then if $f \in L^2(\mathbb{R}^N)$, we have

$$(u^\varepsilon - \theta^\varepsilon) \to 0 \quad \text{in } H^1(\mathbb{R}^N) \tag{17}$$

Furthermore, we have the estimate

$$|u^\varepsilon - \theta^\varepsilon|_{H^1(\mathbb{R}^N)} \leqslant c\varepsilon\|f\|_{L^2(\mathbb{R}^N)} \tag{18}$$

Moreover, because of the analyticity of $\phi_1(\cdot; \eta)$ for $|\eta| \leqslant \delta$ and assuming smooth coefficients $a_{kl}(\cdot)$ in the operator $A$ (which ensure the smoothness of the auxiliary functions $\chi_k, \chi_{kl}$ in (ii)

C. CONCA, S. NATESAN AND M. VANNINATHAN

and (iii) of Theorem 3.3), we can expand it and this give rises to an asymptotic expansion of $\theta^\varepsilon$ which is as follows:

$$\theta^\varepsilon(x) = u^*(x) + \varepsilon\chi_k\left(\frac{x}{\varepsilon}\right)\frac{\partial u^*}{\partial x_k}(x) - \varepsilon^2\left(\chi_{k\ell}\left(\frac{x}{\varepsilon}\right) + \beta_{k\ell}\right)\frac{\partial^2 u^*}{\partial x_k \partial x_\ell}(x) + \cdots$$

where $\beta_{kl}$ are real constants (for details, see statement (iii) in Theorem 3.3 below).

*Theorem 3.3*
Assume that the hypotheses of Theorem 3.2 hold. Then the following statements hold true.

(i) If $u^* \in H^1(\mathbb{R}^N)$, then

$$\|\theta^\varepsilon - u^*\|_{L^2(\mathbb{R}^N)} \leqslant c\varepsilon\|u^*\|_{H^1(\mathbb{R}^N)}$$

(ii) If $f \in L^2(\mathbb{R}^N)$ and $\chi_k \in W_\#^{1,\infty}(Y)$ where $\chi_k$ is the solution of (9) and $\chi_k^\varepsilon(x) = \chi_k(x/\varepsilon)$, then we have

$$\left\|\theta^\varepsilon - u^* - \varepsilon\chi_k^\varepsilon\frac{\partial u^*}{\partial x_k}\right\|_{H^1(\mathbb{R}^N)} \leqslant c\varepsilon\|f\|_{L^2(\mathbb{R}^N)}$$

(iii) If $f \in H^1(\mathbb{R}^N)$ and $\chi_k, \chi_{k\ell} \in W_\#^{1,\infty}(Y)$, then

$$\left\|\theta^\varepsilon - u^* - \varepsilon\chi_k^\varepsilon\frac{\partial u^*}{\partial x_k} + \varepsilon^2(\chi_{k\ell}^\varepsilon + \beta_{k\ell})\frac{\partial^2 u^*}{\partial x_k \partial x_\ell}\right\|_{H^1(\mathbb{R}^N)} \leqslant c\varepsilon^2\|f\|_{H^1(\mathbb{R}^N)}$$

where $\chi_{k\ell}^\varepsilon(x) = \chi_{k\ell}(x/\varepsilon)$, and $\beta_{kl}$ are constants given by $\beta_{k\ell} = \frac{1}{2!}\frac{1}{|Y|}\int_Y \chi_\ell\chi_k\,\mathrm{d}y$.

## 4. NUMERICAL IMPLEMENTATION OF BLOCH WAVES

In this section, we will explain the numerical implementation of the Bloch waves in detail. In the periodic cell $Y$, for the discontinuous coefficients, we have two different regions $Y_0$ and $Y_1$, where the coefficients $a_{kl}$ take different values. Further, in the present case we have to solve the eigenvalue problem (13) for each $\eta \in Y'$. Thus, let us fix $\eta \in Y'$ and consider the following generalized eigenvalue problem

$$-\frac{\partial}{\partial y_k}\left(a_{k\ell}(y)\frac{\partial}{\partial y_\ell}\right)\psi(\cdot;\eta) = \lambda(\eta)\psi(\cdot;\eta) \quad \text{in } Y \tag{19}$$

$$\psi(\cdot;\eta) \text{ is } (\eta, Y)\text{-periodic}$$

The weak formulation of (19) is to find $\psi \in V_\# \stackrel{\text{def}}{=} H_\#^1(\eta; Y)$, such that

$$a(\psi, \zeta) = \lambda(\eta)g(\zeta) \quad \forall \zeta \in V_\# \tag{20}$$

where

$$a(\psi, \zeta) = \int_Y a_{k\ell}\frac{\partial\psi}{\partial y_\ell}\frac{\partial\zeta}{\partial y_k}\,\mathrm{d}y \quad \text{and} \quad g(\zeta) = \int_Y \psi\zeta\,\mathrm{d}y$$

It is easy to see that the bilinear form $a(\cdot, \cdot)$ is elliptic and continuous. A finite element method is obtained by restricting the weak formulation (20) to a finite-dimensional subspace of $V_{\#}$. For $0 \leqslant h \leqslant 1$, let $\mathscr{T}_h$ be a partition of $Y$ by a collection of triangles $T$ with diameter $\leqslant h$, such that

$$\overline{Y} = \bigcup_{T \in \mathscr{T}_h} T$$

Let us define the discretization space $V_h$ as

$$V_h \overset{\text{def}}{=} \{\phi^h \in \mathscr{C}^0(\overline{Y}) : \phi^h \mid_T \in \mathscr{P}_1(T) \quad \forall T \in \mathscr{T}_h\}$$

where $\mathscr{P}_1(T)$ is the space of polynomials of degree at most one. As usual, a basis for $V_h$ is defined by $\{\phi_i, i = 1, \ldots, N_h\}$; $N_h$ being the number of nodes of the partition. Let $(x_j, y_j) \in \overline{Y} (j = 1, \ldots, N_h)$ be a grid point. In addition, we require $\phi_i(x_j, y_j) = \delta_{ij}$. Consider the following discretization subspace $V_{\#h}$ of $V_{\#}$ such that:

$$V_{\#h} \overset{\text{def}}{=} \{\phi^h \in V_h \mid \phi^h \text{ is } (\eta, Y)\text{-periodic}\}$$

The finite element approximation of (20) consists in finding $\psi^h \in V_{\#h}$ such that

$$a(\psi^h, \zeta^h) = \lambda^h(\eta) g(\zeta^h) \quad \forall \zeta^h \in V_{\#h} \tag{21}$$

Conca and Natesan [16] introduced a projection idea to solve elliptic problems (9) and (10) which have $Y$-periodic boundary conditions. More precisely, in order to implement the periodic boundary conditions, the corresponding linear system of the discretized elliptic problem is solved by an iterative method (in particular, the conjugate gradient algorithm) and at each iteration the solution is projected in such a way that for the grid points on the boundary the average of the values on the opposite faces is assigned. In the present case, we have to solve the eigenvalue problem (19) where the boundary conditions are generalized periodic boundary conditions. The main difficulty here is to impose these $(\eta, Y)$-periodic boundary conditions. In order to overcome these difficulties we seek a projection idea similar to the one mentioned above. Here, we cannot just assign the average of values of the grid points on opposite faces, but we have to use an exponential complex weighted average between them. The details are given below.

Let us denote respectively, the discrete interior and the discrete boundary of $Y$ as

$$\text{Int } Y_h = \{(x_j, y_j) \in \overline{Y} \mid 0 < x_j < 2\pi, 0 < y_j < 2\pi\}$$

$$\partial Y_h = \{(x_j, y_j) \in \overline{Y} \mid x_j = 0 \text{ or } 2\pi \quad \text{and} \quad y_j = 0 \text{ or } 2\pi\}$$

The $(\eta, Y)$-periodic projection operator $P_h^\eta : V_h \to V_{\#h}$ is defined as

$$P_h^\eta(v_h) = w_{\#h}^\eta$$

where

$$w_{\#h}^\eta(x_j, y_j) = v_h(x_j, y_j) \quad \text{if } (x_j, y_j) \in \text{Int } Y_h$$

and if $(x_j, y_j)$ is on the boundary $\partial Y_h$, we shall distinguish the following cases:

$$w_{\#h}^\eta(0, y_j) = \mathrm{e}^{-2\pi\mathrm{i}\eta_1} w_{\#h}^\eta(2\pi, y_j) \overset{\text{def}}{=} \tfrac{1}{2}[v_h(0, y_j) + \mathrm{e}^{-2\pi\mathrm{i}\eta_1} v_h(2\pi, y_j)] \tag{22}$$

and

$$w_{\#h}^\eta(x_j, 0) = \mathrm{e}^{-2\pi\mathrm{i}\eta_2} w_{\#h}^\eta(x_j, 2\pi) \overset{\text{def}}{=} \tfrac{1}{2}[v_h(x_j, 0) + \mathrm{e}^{-2\pi\mathrm{i}\eta_2} v_h(x_j, 2\pi)] \tag{23}$$

Observe that with this projection we have for the four corner points,

$$w_{\#h}^\eta(0, 0) = \tfrac{1}{4}[v_h(0, 0) + \mathrm{e}^{-2\pi\mathrm{i}\eta_1} v_h(2\pi, 0) + \mathrm{e}^{-2\pi\mathrm{i}(\eta_1+\eta_2)} v_h(2\pi, 2\pi) + \mathrm{e}^{-2\pi\mathrm{i}\eta_2} v_h(0, 2\pi)]$$

and

$$\mathrm{e}^{-2\pi\mathrm{i}\eta_2} w_{\#h}^\eta(0, 2\pi) = \mathrm{e}^{-2\pi\mathrm{i}\eta_1} w_{\#h}^\eta(2\pi, 0) = \mathrm{e}^{-2\pi\mathrm{i}(\eta_1+\eta_2)} w_{\#h}^\eta(2\pi, 2\pi) = w_{\#h}^\eta(0, 0)$$

For the sake of convenience, let us denote respectively by $\{v_i\}_{i=1}^{N_h}$ and $\{w_i\}_{i=1}^{N_{\#h}}$ the standard finite element basis of $V_h$ and $V_{\#h}$.

The approximate solution $\psi^h$ can be expressed in two different ways, say

$$\psi^h(x, y) = \sum_{i=1}^{N_{\#h}} T_i w_i(x, y) \quad \text{or} \quad \psi^h(x, y) = \sum_{i=1}^{N_h} S_i v_i(x, y)$$

Let $Q$ be the $N_{\#h} \times N_h$ matrix representing the projection operator $P_h^\eta$. Therefore, one can write the problem (21) in the following equivalent form:

$$\begin{aligned} &\text{Find } S \in \mathbb{R}^{N_h}, \ \lambda^h(\eta) \in \mathbb{R} \text{ such that} \\ &AS = \lambda^h(\eta) BS \quad \text{and} \quad Q^t T = S \end{aligned} \tag{24}$$

where $A$ and $B$ are, respectively, the finite element matrices in the space $V_h$ associated with $a(\cdot, \cdot)$ and $g(\cdot)$ as defined in (20). In its turn, (24) can be reduced to the following generalized Sylvester's-type eigenvalue problem:

$$\begin{aligned} &\text{Find } T \in \mathbb{R}^{N_{\#h}}, \ \lambda^h(\eta) \in \mathbb{R} \text{ such that} \\ &CT = \lambda^h(\eta) DT \end{aligned} \tag{25}$$

where $C = QAQ^t$ and $D = QBQ^t$.

From a computational point of view, matrix $Q$ need not be stored in the memory, since matrices $C$ and $D$ can be obtained, respectively, from matrices $A$ and $B$ by means of suitable elementary operations on rows and columns corresponding to the boundary grid points. These elementary operations are nothing but formulas (22) and (23) which define the projection operator $P_h^\eta$ in case of boundary grid points.

In order to determine the homogenized coefficients, we have to find the first (minimum) eigenvalue of the above Sylvester's-type problem in a small neighbourhood of the origin in $Y'$. After finding $\lambda_1$ in a small *ad hoc* grid points around $(0, 0)$, a fourth-order finite difference formula is used to calculate the second derivative of $\lambda_1$ at $\eta = (0, 0)$, which provides the homogenized coefficients as given in (14).

## 4.1. Numerical calculation of the Bloch approximation $\theta^\varepsilon$

We recall the expression of the Bloch approximation $\theta^\varepsilon$:

$$\theta^\varepsilon(x) = \varepsilon^{-N} \int_{Y'} \widehat{u^*}\left(\frac{\eta}{\varepsilon}\right) \mathrm{e}^{\mathrm{i}(x/\varepsilon)\eta} \phi_1\left(\frac{x}{\varepsilon}; \eta\right) \mathrm{d}\eta \qquad (26)$$

Here, the first Bloch eigenvector $\phi_1$ will be approximated by the Sylvester's-type eigenvalue problem (25). In order to obtain $\widehat{u^*}(\eta/\varepsilon)$ explicitly, we shall write the homogenized equation in the Fourier space

$$q_{k\ell} \xi_k \xi_\ell \widehat{u^*}(\xi) + c^* \widehat{u^*}(\xi) = \hat{f}(\xi) \quad \forall \xi \in \mathbb{R}^N$$

Here, the symbol $\widehat{\phantom{x}}$ stands for the classical Fourier transformation

$$\hat{f}(\xi) = \frac{1}{(2\pi)^{N/2}} \int_{\mathbb{R}^N} f(x) \mathrm{e}^{-\mathrm{i}x\xi} \mathrm{d}x$$

More precisely, we have

$$(q_{k\ell}\eta_k\eta_\ell + \varepsilon^2 c^*)\widehat{u^*}\left(\frac{\eta}{\varepsilon}\right) = \varepsilon^2 \hat{f}\left(\frac{\eta}{\varepsilon}\right) \qquad (27)$$

Using (27) in (26), we obtain

$$\theta^\varepsilon(x) = \varepsilon^{2-N} \int_{Y'} \frac{\hat{f}(\frac{\eta}{\varepsilon})}{(q_{k\ell}\eta_k\eta_\ell + \varepsilon^2 c^*)} \mathrm{e}^{\mathrm{i}(x/\varepsilon)\eta} \phi_1\left(\frac{x}{\varepsilon}; \eta\right) \mathrm{d}\eta \quad \forall x \in \mathbb{R}^N \qquad (28)$$

By the use of a quadrature formula one can compute the above integral numerically. Here, we apply a generalization of the Simpson's rule.

The following comments are in order regarding the numerical computation of the integral (28): firstly, it is worthwhile to pointout that $\varepsilon$ though small, is a fixed strictly positive value in our computations with $\theta^\varepsilon(x)$. And hence there is no small denominator problem. Secondly, let us remark about $\hat{f}(\eta/\varepsilon)$: assuming $f$ is smooth, more precisely, if $\hat{f}$ has compact support in $[-K, K]$, then the above integral is restricted to $|\eta| \leqslant K\varepsilon$, for some constant $K$. This poses no difficulty at all. Thirdly, the above expression shows that $\theta^\varepsilon(x)$ in fact depends on $(x/\varepsilon)$. Recall that our attention is focused on the problem localized on $\omega \subset\subset \Omega$. Our aim is to compute $\theta^\varepsilon(x)$ in a fixed finite number of mesh points $x_i$ in $\omega$. Thus, we need to compute the integral (28) at these points $x_i$. Hence, the apparent oscillatory nature of the integral does not pose any further difficulties.

## 4.2. Taylor approximation of $\theta^\varepsilon$

In this section, we propose an approximation for $\theta^\varepsilon$ based on Taylor series expansion for the first Bloch mode $\phi_1$ with respect to $\eta$. To this end, we utilize the properties of $\phi_1$ stated in Theorem 3.1.

Since $\phi_1$ is an analytic function in the Bloch variable $\eta$, one can suggest to replace it in formula (28) by its linear affine approximation at $\eta = 0$. At a first glance this may seem to be little audacious since such a first-order approximation is only accurate in a small neighbourhood of $\eta = 0$, where $\phi_1$ is indeed analytic. However, it is well-known (see Reference [6]) that the

contribution of the components of $\phi_1$ for values of $\eta$ far away from the origin are not so important, i.e. they do not play any important role in the computation of the integral over $Y'$.

More exactly, we propose the following approximation for $\theta^\varepsilon$:

$$\tilde{\theta}^\varepsilon(x) = \varepsilon^{2-N} \int_{Y'} \frac{\hat{f}(\frac{\eta}{\varepsilon})}{(q_{k\ell}\eta_k\eta_\ell + \varepsilon^2 c^*)} e^{i(x/\varepsilon)\eta} \left[ \phi_1\left(\frac{x}{\varepsilon}; 0\right) + \frac{\partial \phi_1}{\partial \eta_k}\left(\frac{x}{\varepsilon}; 0\right)\eta_k \right] d\eta \quad \forall x \in \mathbb{R}^N \qquad (29)$$

If we use the explicit formulas for the first two terms in the right-hand side of (29) given in Theorem 3.1, then we can rewrite $\tilde{\theta}^\varepsilon$ as follows:

$$\tilde{\theta}^\varepsilon(x) = \frac{\varepsilon^{2-N}}{(2\pi)^{N/2}} \int_{Y'} \frac{\hat{f}(\frac{\eta}{\varepsilon})}{(q_{k\ell}\eta_k\eta_\ell + \varepsilon^2 c^*)} e^{i(x/\varepsilon)\eta} \left[ 1 + i\chi_k\left(\frac{x}{\varepsilon}\right)\eta_k \right] d\eta \quad \forall x \in \mathbb{R}^N \qquad (30)$$

The error between $\theta^\varepsilon$ and $\tilde{\theta}^\varepsilon$ are estimated in the following result. As one can see the regularity of the cell solutions with respect to $y \in Y$ does not matter. In fact, this is the essential difference between the Bloch approximation and the classical correctors, namely that $\theta^\varepsilon$ is always in the energy space $H^1(\mathbb{R}^N)$ whereas the classical correctors need not be.

*Theorem 4.1*
Under the hypotheses of Theorem 3.2, we have the following estimates:

$$\|\theta^\varepsilon - \tilde{\theta}^\varepsilon\|_{L^2(\mathbb{R}^N)} \leqslant C\varepsilon^2 \|f\|_{L^2(\mathbb{R}^N)}$$

$$|\theta^\varepsilon - \tilde{\theta}^\varepsilon|_{H^1(\mathbb{R}^N)} \leqslant C\varepsilon \|f\|_{L^2(\mathbb{R}^N)}$$

*Proof*
Applying the results of Theorem 3.1, one can rewrite (28) and (30) by using $\eta = \varepsilon\xi$ as

$$\theta^\varepsilon(x) = \varepsilon^{-N} \int_{\varepsilon^{-1}Y'} \widehat{u^*}(\xi) e^{ix\xi} \phi_1^\varepsilon(x; \xi) d\xi$$

where we recall $\phi_1^\varepsilon(x; \xi) = \phi_1(x/\varepsilon; \varepsilon\xi)$, and

$$\tilde{\theta}^\varepsilon(x) = \varepsilon^{-N} \int_{\varepsilon^{-1}Y'} \widehat{u^*}(\xi) e^{ix\xi} \left[ \phi_1\left(\frac{x}{\varepsilon}; 0\right) + \varepsilon\xi_k \frac{\partial \phi_1}{\partial \eta_k}\left(\frac{x}{\varepsilon}; 0\right) \right] d\xi$$

By subtraction, we get

$$\theta^\varepsilon(x) - \tilde{\theta}^\varepsilon(x) = \varepsilon^{-N} \int_{|\xi| \leqslant \delta\varepsilon^{-1}} \widehat{u^*}(\xi) e^{ix\xi} \left[ \phi_1^\varepsilon(x; \xi) - \phi_1\left(\frac{x}{\varepsilon}; 0\right) - \varepsilon\xi_k \frac{\partial \phi_1}{\partial \eta_k}\left(\frac{x}{\varepsilon}; 0\right) \right] d\xi$$

$$+ \varepsilon^{-N} \int_{\substack{\xi \in \varepsilon^{-1}Y' \\ |\xi| > \delta\varepsilon^{-1}}} \widehat{u^*}(\xi) e^{ix\xi} \phi_1^\varepsilon(x; \xi) d\xi$$

$$- \varepsilon^{-N} \int_{\substack{\xi \in \varepsilon^{-1}Y' \\ |\xi| > \delta\varepsilon^{-1}}} \widehat{u^*}(\xi) e^{ix\xi} \left[ \phi_1\left(\frac{x}{\varepsilon}; 0\right) + \varepsilon\xi_k \frac{\partial \phi_1}{\partial \eta_k}\left(\frac{x}{\varepsilon}; 0\right) \right] d\xi \qquad (31)$$

Now applying Lemma 2.3 of Reference [6], we have

$$\|\theta^\varepsilon - \tilde{\theta}^\varepsilon\|^2_{L^2(\mathbb{R}^N)} \leqslant \int_{|\xi| \leqslant \delta\varepsilon^{-1}} |\widehat{u^*}(\xi)|^2 \left\| \phi_1(y; \varepsilon\xi) - \phi_1(y; 0) - \varepsilon\xi_k \frac{\partial\phi_1}{\partial\eta_k}(y; 0) \right\|^2_{L^2(Y)} \mathrm{d}\xi$$

$$+ \int_{\substack{\xi \in \varepsilon^{-1}Y' \\ |\xi| > \delta\varepsilon^{-1}}} |\widehat{u^*}(\xi)|^2 \|\phi_1(y; \varepsilon\xi)\|^2_{L^2(Y)} \mathrm{d}\xi$$

$$+ \int_{\substack{\xi \in \varepsilon^{-1}Y' \\ |\xi| > \delta\varepsilon^{-1}}} |\widehat{u^*}(\xi)|^2 \left\| \phi_1(y; 0) + \varepsilon\xi_k \frac{\partial\phi_1}{\partial\eta_k}(y; 0) \right\|^2_{L^2(Y)} \mathrm{d}\xi$$

Using Theorem 3.1, and recalling that we have normalized the $L^2$–norm of $\phi_1(\cdot; \eta)$ to unity, we get

$$\|\theta^\varepsilon - \tilde{\theta}^\varepsilon\|^2_{L^2(\mathbb{R}^N)} \leqslant C \int_{|\xi| \leqslant \delta\varepsilon^{-1}} |\widehat{u^*}(\xi)|^2 (\varepsilon^2|\xi|^2)^2 \, \mathrm{d}\xi + \int_{\substack{\xi \in \varepsilon^{-1}Y' \\ |\xi| > \delta\varepsilon^{-1}}} |\widehat{u^*}(\xi)|^2 \, \mathrm{d}\xi$$

$$+ C \int_{\substack{\xi \in \varepsilon^{-1}Y' \\ |\xi| > \delta\varepsilon^{-1}}} |\widehat{u^*}(\xi)|^2 \, \mathrm{d}\xi$$

Therefore,

$$\|\theta^\varepsilon - \tilde{\theta}^\varepsilon\|^2_{L^2(\mathbb{R}^N)} \leqslant C\varepsilon^4 \int_{\mathbb{R}^N} |\xi|^4 |\widehat{u^*}(\xi)|^2 \, \mathrm{d}\xi + C \int_{|\xi| > \delta\varepsilon^{-1}} |\widehat{u^*}(\xi)|^2 \, \mathrm{d}\xi$$

$$\leqslant C\varepsilon^4 \int_{\mathbb{R}^N} |\xi|^4 |\widehat{u^*}(\xi)|^2 \, \mathrm{d}\xi + C\delta^{-4}\varepsilon^4 \int_{\mathbb{R}^N} |\xi|^4 |\widehat{u^*}(\xi)|^2 \, \mathrm{d}\xi$$

$$\leqslant C\varepsilon^4 \|u^*\|^2_{H^2(\mathbb{R}^N)}$$

$$\leqslant C\varepsilon^4 \|f\|^2_{L^2(\mathbb{R}^N)}$$

Again applying Lemma 2.3 from Reference [6] to the expression (31), we obtain

$$|\theta^\varepsilon - \tilde{\theta}^\varepsilon|^2_{H^1(\mathbb{R}^N)} \leqslant \int_{|\xi| \leqslant \delta\varepsilon^{-1}} |\widehat{u^*}(\xi)|^2 \|\mathrm{i}\xi\rho(y, \varepsilon\xi) + \varepsilon^{-1}\nabla_y\rho(y, \varepsilon\xi)\|^2_{L^2(Y)} \mathrm{d}\xi$$

$$+ \int_{\substack{\xi \in \varepsilon^{-1}Y' \\ |\xi| > \delta\varepsilon^{-1}}} |\widehat{u^*}(\xi)|^2 \|\mathrm{i}\xi\phi_1(y; \varepsilon\xi) + \varepsilon^{-1}\nabla_y\phi_1(y; \varepsilon\xi)\|^2_{L^2(Y)} \mathrm{d}\xi$$

$$+ \int_{\substack{\xi \in \varepsilon^{-1}Y' \\ |\xi| > \delta\varepsilon^{-1}}} |\widehat{u^*}(\xi)|^2 \|\mathrm{i}\xi\rho_R(y, \varepsilon\xi) + \varepsilon^{-1}\nabla_y\rho_R(y, \varepsilon\xi)\|^2_{L^2(Y)} \mathrm{d}\xi$$

where

$$\rho(y, \eta) = \phi_1(y; \eta) - \phi_1(y; 0) - \eta_k \frac{\partial \phi_1}{\partial \eta_k}(y; 0)$$

$$\rho_R(y, \eta) = \phi_1(y; 0) + \eta_k \frac{\partial \phi_1}{\partial \eta_k}(y; 0)$$

Using the estimates

$$\|\rho(y, \eta)\|_{L^2(Y)} + \|\nabla_y \rho(y, \eta)\|_{L^2(Y)} = O(|\eta|^2) \quad \text{for } |\eta| \leqslant \delta$$

$$\|\rho_R(y, \eta)\|_{L^2(Y)} + \|\nabla_y \rho_R(y, \eta)\|_{L^2(Y)} \leqslant C \quad \text{for } y \in Y'$$

we obtain

$$|\theta^\varepsilon - \tilde{\theta}^\varepsilon|^2_{H^1(\mathbb{R}^N)} \leqslant C\varepsilon^2 \int_{\mathbb{R}^N} |\widehat{u^*}(\xi)|^2 |\xi|^4 \, \mathrm{d}\xi$$

$$\leqslant C\varepsilon^2 \|u^*\|^2_{H^2(\mathbb{R}^N)}$$

$$\leqslant C\varepsilon^2 \|f\|^2_{L^2(\mathbb{R}^N)}$$

This finishes the proof. □

It is more easy to implement $\tilde{\theta}^\varepsilon$ numerically than $\theta^\varepsilon$ because the auxiliary function $\chi_k$ is much easier to compute numerically than $\phi_1$. The computation of $\chi_k$ can be done either by solving problem (9) directly or by evaluating the left-hand side of (15) numerically. We will see later in Section 5 that this simpler approximation $\tilde{\theta}^\varepsilon$ of $\theta^\varepsilon$ performs numerically as well as the classical first-order corrector term.

## 5. NUMERICAL EXAMPLES

In this section, we provide exhaustive numerical examples in one and two dimensions supporting our claims in the previous sections. We apply the Bloch approximation for both the smooth and discontinuous coefficient cases. For the calculation of the homogenized coefficients and the determination of $\chi_k$'s by both classical and Bloch methods and the classical first- and second-order correctors, one can refer to Reference [16] (in this paper, the authors also provided a comparison between the exact solution $u^\varepsilon$ and these classical approximations).

### 5.1. One-dimensional case

*Example 5.1* (*The discontinuous coefficients case*)
Consider the following one-dimensional boundary-value problem:

$$-\frac{\mathrm{d}}{\mathrm{d}x}\left(a\left(\frac{x}{\varepsilon}\right)\frac{\mathrm{d}u^\varepsilon}{\mathrm{d}x}(x)\right) + u^\varepsilon(x) = \frac{\sin x}{x}, \quad x \in \Omega = \, ]-2\pi, 2\pi[ \tag{32}$$

$$u^\varepsilon(-2\pi) = 0, \quad u^\varepsilon(2\pi) = 0$$

where $a(x/\varepsilon)$ is the oscillating coefficient.

Table I. Homogenized coefficient for Example 5.1.

| $a_0$ | Bloch method | Classical method | Difference |
|---|---|---|---|
| 1/18 | 0.1500 | 0.1500 | 2.6676e-07 |
| 1/114 | 0.0259 | 0.0259 | 5.9477e-08 |

Table II. Homogenized coefficient for Example 5.2.

| Bloch method | Classical method | Difference |
|---|---|---|
| 1.7322 | 1.7322 | 5.0131e-07 |

As a first step, we shall determine the homogenized coefficient and then $\chi$ (where $\chi = \chi_k$ corresponds to one-dimensional version of $\chi_k$) by the Bloch method. To this end, let us consider the following problem in the periodic cell $Y = ]0, 2\pi[$:

$$-\frac{\mathrm{d}}{\mathrm{d}y}\left(a(y)\frac{\mathrm{d}\psi}{\mathrm{d}y}(y;\eta)\right) = \lambda(\eta)\psi(y;\eta), \quad y \in Y, \quad \eta \in Y' = \left]-\frac{1}{2},\frac{1}{2}\right[$$

(33)

$$\psi(\cdot;\eta) \text{ is } (\eta, Y)\text{-periodic}$$

where

$$a(y) = \begin{cases} a_0 & \text{in } Y_1 \stackrel{\text{def}}{=} \left(\frac{2\pi}{3}, \frac{4\pi}{3}\right) \\ 1 & \text{in } Y_0 \stackrel{\text{def}}{=} Y \setminus Y_1 \end{cases}$$

and we consider two different values for $a_0$ as $a_0 = 1/18$ and $1/114$ which were obtained from physical applications for the two-dimensional case in Reference [17].

Table I gives the computed homogenized coefficients by classical (i.e. (12)) and Bloch methods (i.e. (14)) and their respective differences.

*Example 5.2* (*The continuous coefficient case*)
Consider the problem as given in Example 5.1 with the following smooth coefficients:

$$a(y) = 2 + \cos(y) \quad \text{or} \quad a(y) = 2 + \sin(y)$$

The homogenized coefficient computed by both the classical and Bloch methods is given in Table II.

*5.1.1. Comparison of $\theta^\varepsilon$ with $u^\varepsilon$ and the first-order corrector.* In this section, we make a comparative study between the Bloch approximation $\theta^\varepsilon$, the exact solution $u^\varepsilon$ and the classical first-order corrector term which is given as follows:

$$v_1^\varepsilon(x) = u^*(x) + \varepsilon\chi\left(\frac{x}{\varepsilon}\right)\frac{\mathrm{d}u^*}{\mathrm{d}x}(x)$$

where $u^*$ is the solution of the homogenized problem (11).

We plotted $\theta^\varepsilon$, $u^\varepsilon$ and $v_1^\varepsilon$ respectively in broken, solid and dotted lines in Figures 1 and 2. These figures plot $\theta^\varepsilon$, $u^\varepsilon$ and $v_1^\varepsilon$, inside the main peak which was obtained by zooming in small different intervals around the origin. From these plots one can easily see that the Bloch approximation $\theta^\varepsilon$ is closer to $u^\varepsilon$ than the classical first-order corrector $v_1^\varepsilon$ which justifies our claim in Section 4.1.

More precisely, we have indicated in Table IV the errors $(u^\varepsilon - \theta^\varepsilon)$, $(u^\varepsilon - v_1^\varepsilon)$ and $(\theta^\varepsilon - v_1^\varepsilon)$ in the norms of the spaces $L^2(\omega)$, $L^\infty(\omega)$ and $H^1(\omega)$, $W^{1,\infty}(\omega)$ where $\omega = [-\pi, \pi]$. Here, we have compared these differences only in $\omega$ instead of the full domain $\Omega = ]-2\pi, 2\pi[$. This is because the Bloch approximation $\theta^\varepsilon$ is theoretically valid in the absence of boundaries. Therefore, in the case of bounded domains, a fair comparison between $\theta^\varepsilon$ and $v_1^\varepsilon$ should consist in comparing a local norm or semi-norm for $(u^\varepsilon - \theta^\varepsilon)$ and $(u^\varepsilon - v_1^\varepsilon)$, and this has been done
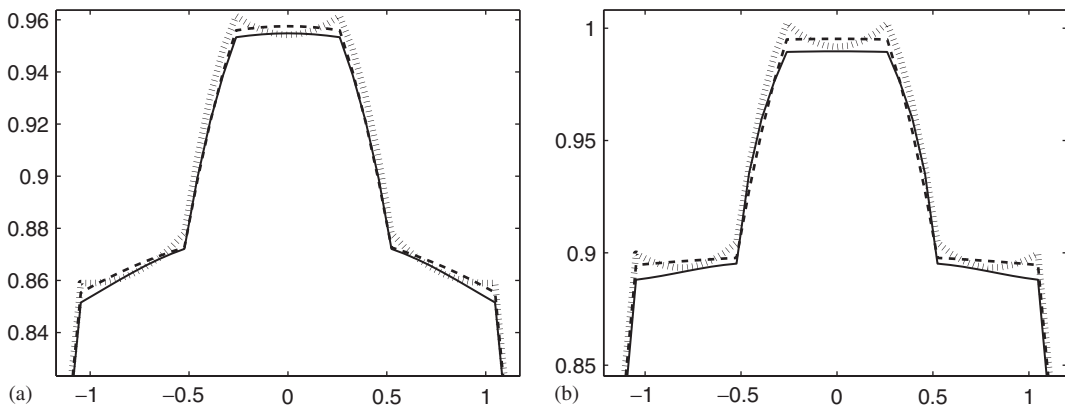


Figure 1. $u^\varepsilon$, $\theta^\varepsilon$ and $v_1^\varepsilon$ for $\varepsilon = 1/8$ (Example 5.1): (a) for $a_0 = 1/18$; and (b) for $a_0 = 1/114$.
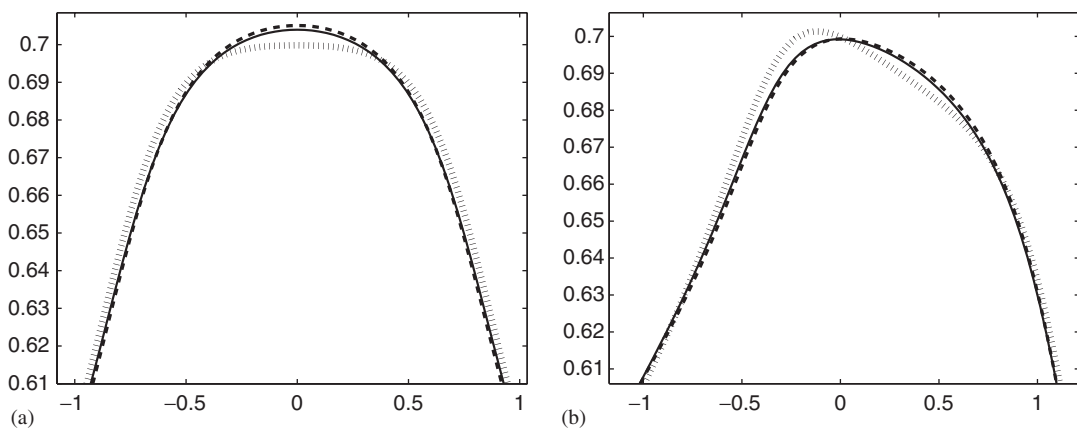


Figure 2. $u^\varepsilon$, $\theta^\varepsilon$ and $v_1^\varepsilon$ for $\varepsilon = 1/4$ (Example 5.2): (a) for $a(y) = 2 + \cos(y)$; and (b) for $a(y) = 2 + \sin(y)$.

Table III. Convergence of the error for $a_0 = 1/18$ inside a peak (Example 5.1).

| $\varepsilon$ | $\dfrac{\|u^\varepsilon-\theta^\varepsilon\|_{L^\infty(\cdot)}}{\|u^\varepsilon\|_{L^\infty(\cdot)}}$ | $\dfrac{\|u^\varepsilon-v_1^\varepsilon\|_{L^\infty(\cdot)}}{\|u^\varepsilon\|_{L^\infty(\cdot)}}$ | $\dfrac{\|\theta^\varepsilon-v_1^\varepsilon\|_{L^\infty(\cdot)}}{\|u^\varepsilon\|_{L^\infty(\cdot)}}$ | $\dfrac{\|(u^\varepsilon-\theta^\varepsilon)'\|_{L^\infty(\cdot)}}{\|(u^\varepsilon)'\|_{L^\infty(\cdot)}}$ | $\dfrac{\|(u^\varepsilon-v_1^\varepsilon)'\|_{L^\infty(\cdot)}}{\|(u^\varepsilon)'\|_{L^\infty(\cdot)}}$ | $\dfrac{\|(\theta^\varepsilon-v_1^\varepsilon)'\|_{L^\infty(\cdot)}}{\|(u^\varepsilon)'\|_{L^\infty(\cdot)}}$ |
|---|---|---|---|---|---|---|
| 1/2 | 0.1100 | 0.1773 | 0.0937 | 0.6994 | 0.7299 | 0.3013 |
| 1/4 | 0.0180 | 0.0393 | 0.0386 | 0.3009 | 0.2591 | 0.2597 |
| 1/8 | 0.0029 | 0.0106 | 0.0103 | 0.0857 | 0.2156 | 0.2183 |
| 1/16 | 5.9840e-04 | 0.0030 | 0.0026 | 0.0205 | 0.2003 | 0.2008 |
| 1/32 | 1.3878e-04 | 7.7794e-04 | 6.5144e-04 | 0.0054 | 0.1987 | 0.1987 |
| 1/64 | 3.2204e-05 | 1.9717e-04 | 1.6585e-04 | 0.0015 | 0.2039 | 0.2038 |
| 1/128 | 6.5266e-06 | 4.1346e-05 | 3.4824e-05 | 2.2005e-04 | 0.0036 | 0.0036 |
| 1/256 | 1.4480e-07 | 1.0338e-05 | 1.0193e-05 | 2.3642e-04 | 0.2664 | 0.2662 |

Table IV. Convergence of the error for $a_0 = 1/114$ (Example 5.1).

| $\varepsilon$ | $\dfrac{\|u^\varepsilon-\theta^\varepsilon\|_{L^\infty(\omega)}}{\|u^\varepsilon\|_{L^\infty(\omega)}}$ | $\dfrac{\|u^\varepsilon-v_1^\varepsilon\|_{L^\infty(\omega)}}{\|u^\varepsilon\|_{L^\infty(\omega)}}$ | $\dfrac{\|\theta^\varepsilon-v_1^\varepsilon\|_{L^\infty(\omega)}}{\|u^\varepsilon\|_{L^\infty(\omega)}}$ | $\dfrac{\|(u^\varepsilon-\theta^\varepsilon)'\|_{L^\infty(\omega)}}{\|(u^\varepsilon)'\|_{L^\infty(\omega)}}$ | $\dfrac{\|(u^\varepsilon-v_1^\varepsilon)'\|_{L^\infty(\omega)}}{\|(u^\varepsilon)'\|_{L^\infty(\omega)}}$ | $\dfrac{\|(\theta^\varepsilon-v_1^\varepsilon)'\|_{L^\infty(\omega)}}{\|(u^\varepsilon)'\|_{L^\infty(\omega)}}$ |
|---|---|---|---|---|---|---|
| 1/2 | 0.3085 | 0.2806 | 0.1166 | 0.6256 | 0.5332 | 0.0904 |
| 1/4 | 0.0820 | 0.0792 | 0.0468 | 0.4548 | 0.3826 | 0.0180 |
| 1/8 | 0.0144 | 0.0169 | 0.0126 | 0.1703 | 0.1586 | 0.0509 |
| 1/16 | 0.0020 | 0.0037 | 0.0032 | 0.0698 | 0.0665 | 0.0294 |
| 1/32 | 3.0368e-04 | 9.4969e-04 | 7.9651e-04 | 0.0168 | 0.0199 | 0.0153 |
| 1/64 | 5.3088e-05 | 2.3830e-04 | 2.0121e-04 | 0.0034 | 0.0075 | 0.0075 |
| 1/128 | 1.8571e-05 | 5.0985e-05 | 5.0629e-05 | 8.6563e-04 | 0.0038 | 0.0038 |
| 1/256 | 1.6713e-05 | 1.2661e-05 | 1.7460e-05 | 2.4559e-04 | 0.0019 | 0.0019 |

Table V. Convergence of the error for Example 5.2 inside a peak.

| $\varepsilon$ | $\dfrac{\|u^\varepsilon-\theta^\varepsilon\|_{L^\infty(\cdot)}}{\|u^\varepsilon\|_{L^\infty(\cdot)}}$ | $\dfrac{\|u^\varepsilon-v_1^\varepsilon\|_{L^\infty(\cdot)}}{\|u^\varepsilon\|_{L^\infty(\cdot)}}$ | $\dfrac{\|\theta^\varepsilon-v_1^\varepsilon\|_{L^\infty(\cdot)}}{\|u^\varepsilon\|_{L^\infty(\cdot)}}$ | $\dfrac{\|(u^\varepsilon-\theta^\varepsilon)'\|_{L^\infty(\cdot)}}{\|(u^\varepsilon)'\|_{L^\infty(\cdot)}}$ | $\dfrac{\|(u^\varepsilon-v_1^\varepsilon)'\|_{L^\infty(\cdot)}}{\|(u^\varepsilon)'\|_{L^\infty(\cdot)}}$ | $\dfrac{\|(\theta^\varepsilon-v_1^\varepsilon)'\|_{L^\infty(\cdot)}}{\|(u^\varepsilon)'\|_{L^\infty(\cdot)}}$ |
|---|---|---|---|---|---|---|
| 1/2 | 0.0339 | 0.0201 | 0.0496 | 0.1897 | 0.0989 | 0.1535 |
| 1/4 | 0.0016 | 0.0058 | 0.0075 | 0.0425 | 0.1589 | 0.1811 |
| 1/8 | 4.5950e-04 | 0.0027 | 0.0025 | 0.0096 | 0.1028 | 0.1084 |
| 1/16 | 6.4114e-05 | 7.0494e-04 | 6.5752e-04 | 0.0028 | 0.1020 | 0.1033 |
| 1/32 | 6.0134e-05 | 2.4465e-04 | 1.8629e-04 | 0.0016 | 0.1023 | 0.1029 |
| 1/64 | 5.8449e-05 | 1.2637e-04 | 6.8219e-05 | 0.0014 | 0.1023 | 0.1029 |

by computing the above norm/semi-norm in a relatively compact domain $\omega$ in $\Omega$. Moreover, the above-mentioned errors are also presented inside the main peak of $u^\varepsilon$. They are denoted by $(\cdot)$ in Tables III and V. Here, the above norm/semi-norm measures the relative errors in a local subdomain.

### 5.1.2. Comparison of $\theta^\varepsilon$ with $u^\varepsilon$ and the second-order corrector. 
This section presents the comparison results between the Bloch approximation $\theta^\varepsilon$, the exact solution $u^\varepsilon$ and the classical

second-order corrector term given by

$$v_2^\varepsilon(x) = u^*(x) + \varepsilon\chi\left(\frac{x}{\varepsilon}\right)\frac{\mathrm{d}u^*}{\mathrm{d}x}(x) - \varepsilon^2\zeta\left(\frac{x}{\varepsilon}\right)\frac{\mathrm{d}^2u^*}{\mathrm{d}x^2}(x)$$

where $\zeta$ corresponds to one-dimensional version of $\chi_{k\ell}$, solution of the cell problem (10).

In Figures 3 and 4, we have plotted the zoomed main peak of $\theta^\varepsilon$, $u^\varepsilon$ and $v_2^\varepsilon$, respectively, in broken, solid, and dotted lines for different values of $\varepsilon$. One can easily notice that the accuracy of the Bloch approximation function $\theta^\varepsilon$. The Bloch approximation function $\theta^\varepsilon$ approximates the exact solution better than the classical second-order corrector. More precisely, for high-contrast material, $v_2^\varepsilon$ exhibits spurious oscillations whereas $\theta^\varepsilon$ does not do so and provides a better
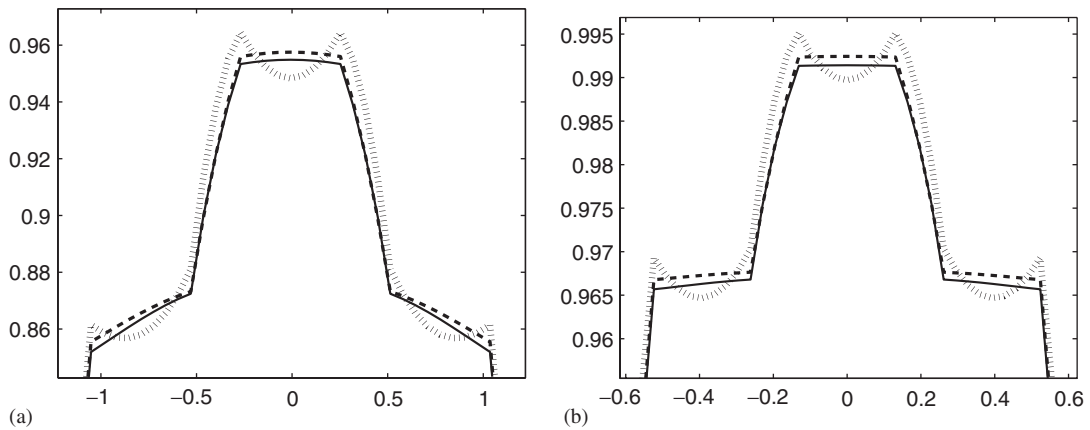


Figure 3. $u^\varepsilon$, $\theta^\varepsilon$ and $v_2^\varepsilon$ (Example 5.1): (a) for $a_0 = 1/18$ and $\varepsilon = 1/8$; and (b) for $a_0 = 1/114$ and $\varepsilon = 1/16$.



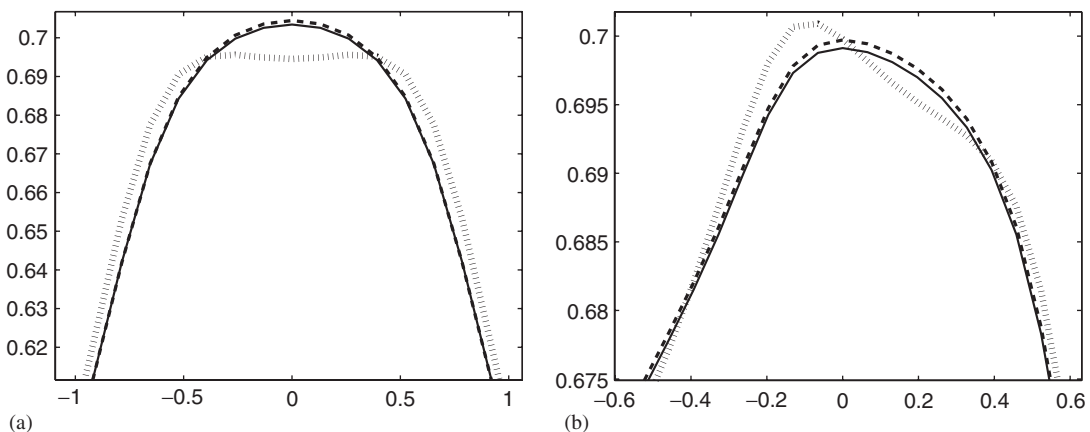Figure 4. $u^\varepsilon$, $\theta^\varepsilon$ and $v_2^\varepsilon$ (Example 5.2): (a) for $a(y) = 2 + \cos(y)$ and $\varepsilon = 1/4$; and (b) for $a(y) = 2 + \sin(y)$ and $\varepsilon = 1/8$.

Table VI. Convergence of the error for $a_0 = 1/18$ (Example 5.1).

| $\varepsilon$ | $\frac{\|u^\varepsilon-\theta^\varepsilon\|_{L^\infty(\omega)}}{\|u^\varepsilon\|_{L^\infty(\omega)}}$ | $\frac{\|u^\varepsilon-v_2^\varepsilon\|_{L^\infty(\omega)}}{\|u^\varepsilon\|_{L^\infty(\omega)}}$ | $\frac{\|\theta^\varepsilon-v_2^\varepsilon\|_{L^\infty(\omega)}}{\|u^\varepsilon\|_{L^\infty(\omega)}}$ | $\frac{\|(u^\varepsilon-\theta^\varepsilon)'\|_{L^\infty(\omega)}}{\|(u^\varepsilon)'\|_{L^\infty(\omega)}}$ | $\frac{\|(u^\varepsilon-v_2^\varepsilon)'\|_{L^\infty(\omega)}}{\|(u^\varepsilon)'\|_{L^\infty(\omega)}}$ | $\frac{\|(\theta^\varepsilon-v_2^\varepsilon)'\|_{L^\infty(\omega)}}{\|(u^\varepsilon)'\|_{L^\infty(\omega)}}$ |
|---|---|---|---|---|---|---|
| 1/2 | 0.1603 | 0.1809 | 0.1373 | 0.3091 | 0.4073 | 0.2964 |
| 1/4 | 0.0284 | 0.0559 | 0.0619 | 0.1600 | 0.1972 | 0.2000 |
| 1/8 | 0.0040 | 0.0173 | 0.0176 | 0.0491 | 0.1062 | 0.1068 |
| 1/16 | 6.6736e-04 | 0.0049 | 0.0045 | 0.0125 | 0.0542 | 0.0543 |
| 1/32 | 1.3167e-04 | 0.0013 | 0.0012 | 0.0031 | 0.0273 | 0.0273 |
| 1/64 | 5.7495e-05 | 3.1876e-04 | 2.9438e-04 | 8.0192e-04 | 0.0137 | 0.0137 |
| 1/128 | 5.2075e-05 | 7.9850e-05 | 8.1661e-05 | 2.4375e-04 | 0.0068 | 0.0068 |
| 1/256 | 5.2017e-05 | 1.9972e-05 | 5.5376e-05 | 2.1474e-04 | 0.0034 | 0.0034 |

Table VII. Convergence of the error for $a_0 = 1/114$ (Example 5.1).

| $\varepsilon$ | $\frac{\|u^\varepsilon-\theta^\varepsilon\|_{L^2(\omega)}}{\|u^\varepsilon\|_{L^2(\omega)}}$ | $\frac{\|u^\varepsilon-v_2^\varepsilon\|_{L^2(\omega)}}{\|u^\varepsilon\|_{L^2(\omega)}}$ | $\frac{\|\theta^\varepsilon-v_2^\varepsilon\|_{L^2(\omega)}}{\|u^\varepsilon\|_{L^2(\omega)}}$ | $\frac{|u^\varepsilon-\theta^\varepsilon|_{H^1(\omega)}}{|u^\varepsilon|_{H^1(\omega)}}$ | $\frac{|u^\varepsilon-v_2^\varepsilon|_{H^1(\omega)}}{|u^\varepsilon|_{H^1(\omega)}}$ | $\frac{|\theta^\varepsilon-v_2^\varepsilon|_{H^1(\omega)}}{|u^\varepsilon|_{H^1(\omega)}}$ |
|---|---|---|---|---|---|---|
| 1/2 | 0.1946 | 0.2005 | 0.1426 | 0.3758 | 0.5143 | 0.3156 |
| 1/4 | 0.0488 | 0.0506 | 0.0449 | 0.3589 | 0.3450 | 0.1944 |
| 1/8 | 0.0081 | 0.0119 | 0.0111 | 0.1295 | 0.1425 | 0.0946 |
| 1/16 | 0.0012 | 0.0030 | 0.0028 | 0.0391 | 0.0561 | 0.0472 |
| 1/32 | 2.1012e-04 | 7.5933e-04 | 6.9968e-04 | 0.0087 | 0.0245 | 0.0235 |
| 1/64 | 6.1423e-05 | 1.8722e-04 | 1.8628e-04 | 0.0025 | 0.0116 | 0.0116 |
| 1/128 | 5.6832e-05 | 4.3497e-05 | 7.3982e-05 | 6.5696e-04 | 0.0059 | 0.0059 |
| 1/256 | 5.9480e-05 | 1.1468e-05 | 5.8765e-05 | 2.0556e-04 | 0.0028 | 0.0031 |

Table VIII. Convergence of the error for Example 5.2.

| $\varepsilon$ | $\frac{\|u^\varepsilon-\theta^\varepsilon\|_{L^\infty(\omega)}}{\|u^\varepsilon\|_{L^\infty(\omega)}}$ | $\frac{\|u^\varepsilon-v_2^\varepsilon\|_{L^\infty(\omega)}}{\|u^\varepsilon\|_{L^\infty(\omega)}}$ | $\frac{\|\theta^\varepsilon-v_2^\varepsilon\|_{L^\infty(\omega)}}{\|u^\varepsilon\|_{L^\infty(\omega)}}$ | $\frac{\|(u^\varepsilon-\theta^\varepsilon)'\|_{L^\infty(\omega)}}{\|(u^\varepsilon)'\|_{L^\infty(\omega)}}$ | $\frac{\|(u^\varepsilon-v_2^\varepsilon)'\|_{L^\infty(\omega)}}{\|(u^\varepsilon)'\|_{L^\infty(\omega)}}$ | $\frac{\|(\theta^\varepsilon-v_2^\varepsilon)'\|_{L^\infty(\omega)}}{\|(u^\varepsilon)'\|_{L^\infty(\omega)}}$ |
|---|---|---|---|---|---|---|
| 1/2 | 0.0467 | 0.0467 | 0.0823 | 0.1750 | 0.1470 | 0.1998 |
| 1/4 | 0.0036 | 0.0161 | 0.0176 | 0.0291 | 0.1013 | 0.0999 |
| 1/8 | 5.5321e-04 | 0.0053 | 0.0047 | 0.0060 | 0.0557 | 0.0578 |
| 1/16 | 1.6984e-04 | 0.0020 | 0.0012 | 0.0024 | 0.0285 | 0.0289 |
| 1/32 | 1.6169e-04 | 0.0012 | 3.4480e-04 | 9.1081e-04 | 0.0146 | 0.0145 |
| 1/64 | 1.8913e-04 | 9.4895e-04 | 1.3306e-04 | 0.0013 | 0.0077 | 0.0072 |

approximation for $u^\varepsilon$. One can note this from the Figures 3 and 4. Further, we have presented the errors in different norms in Tables VI–VIII.

In order to make a comparison between the computational costs of the Bloch approximation function $\theta^\varepsilon$, the exact solution and the classical first- and second-order correctors, we determined the CPU time for each of these. (The CPU times for the computation of the solutions of the cell problems $\chi$ and $\zeta$, and the first Bloch eigenvector $\phi_1(\cdot; \eta)$ are excluded, because they are independent of $\varepsilon$ and they are computed once and for all). The CPU times for these quantities are presented in Table IX in seconds. The computations are carried out in a Pentium III processor machine with 256 MB RAM and 500 MHz speed by using MATLAB. The number of mesh points used in the domain $[-2\pi, 2\pi]$ for each case is $2 \times 3 \times 4/\varepsilon$. From Table IX one can

Table IX. CPU time for the exact solution, classical correctors (in s).

| $\varepsilon$ | Exact solution | I-order corr. | II-order corr. |
|------|------|------|------|
| 1/2 | 0.2436 | 0.2339 | 0.2423 |
| 1/4 | 0.3894 | 0.2790 | 0.2812 |
| 1/8 | 0.6035 | 0.3931 | 0.4282 |
| 1/16 | 1.2297 | 0.7899 | 0.8427 |
| 1/32 | 2.5929 | 1.6650 | 1.8604 |
| 1/64 | 5.9308 | 4.4521 | 4.7894 |
| 1/128 | 15.1811 | 12.9359 | 13.3080 |

Table X. CPU time for $\theta^{\varepsilon}$ on coarse grids (in s).

| $\varepsilon$ | 384 pts. | 768 pts. | 1536 pts. |
|------|------|------|------|
| 1/2 | 4.4623 | 8.4217 | 18.1725 |
| 1/4 | 4.7851 | 9.3473 | 19.2634 |
| 1/8 | 4.6289 | 9.5624 | 18.5851 |
| 1/16 | 5.0127 | 8.9843 | 19.1099 |
| 1/32 | 4.8912 | 9.0169 | 18.6723 |
| 1/64 | 5.2178 | 8.7603 | 18.7328 |
| 1/128 | 4.9012 | 9.2085 | 19.1729 |

note that as $\varepsilon$ decreases, the CPU time for $v_2^{\varepsilon}$ increases by a factor of 3 whereas it is steady in the case of $\theta^{\varepsilon}$. Thus, though initially the number of operations for $\theta^{\varepsilon}$ is more than that of $v_2^{\varepsilon}$, it is clearly going to be the other way round when $\varepsilon$ is small. For instance, if $\varepsilon = 1/256$, the CPU times for $v_2^{\varepsilon}$ and $\theta^{\varepsilon}$ would be around 39 and 19, respectively. Thus, we gain appreciable CPU time for smaller values of $\varepsilon$ (Table X).

*5.1.3. Comparison of $\tilde{\theta}^{\varepsilon}$ with $u^{\varepsilon}$ and $v_1^{\varepsilon}$.* This section reports a comparative analysis between the Taylor approximation function $\tilde{\theta}^{\varepsilon}$ of the Bloch approximation function $\theta^{\varepsilon}$ and the exact solution $u^{\varepsilon}$, the classical first-order corrector $v_1^{\varepsilon}$ in terms of figures and numerical tables.

As mentioned earlier the Taylor approximation function $\tilde{\theta}^{\varepsilon}$ provides almost the same approximate value to $u^{\varepsilon}$ as the first-order corrector term $v_1^{\varepsilon}$. Hence, it is difficult to distinguish between both $\tilde{\theta}^{\varepsilon}$ and $v_1^{\varepsilon}$ in the plots. In order to make it easy to the readers, only the *difference* between both functions is plotted in Figure 5.

In addition, we have also compared both functions with $u^{\varepsilon}$ in different local norms and presented the relative errors in Tables XI–XIII.

*5.2. Two-dimensional case*

In this section, we compute the Bloch approximation function $\theta^{\varepsilon}$ and its Taylor approximation $\tilde{\theta}^{\varepsilon}$ for two-dimensional examples. We performed the comparison between the classical first- and second-order correctors with these two new approximation functions. The results are presented in the form of tables and figures.
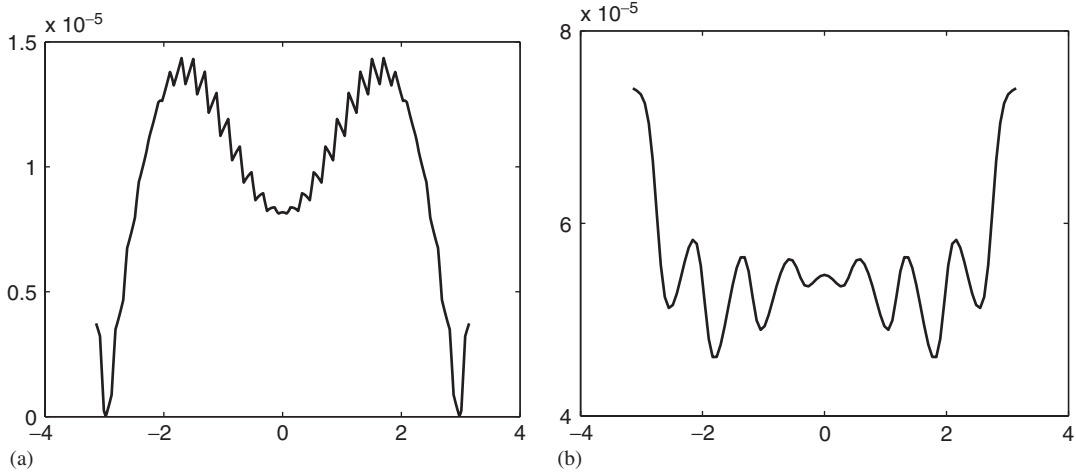
Figure 5. $|\tilde{\theta}^{\varepsilon} - v_1^{\varepsilon}|$ inside $\omega = ]-\pi, \pi[$: (a) for $a_0 = 1/18$ and $\varepsilon = 1/32$; and (b) for $a(y) = 2 + \cos(y)$ and $\varepsilon = 1/8$.

Table XI. Convergence of the error for $a_0 = 1/18$ (Example 5.1).

| $\varepsilon$ | $\dfrac{\|u^{\varepsilon}-\tilde{\theta}^{\varepsilon}\|_{L^{\infty}(\omega)}}{\|u^{\varepsilon}\|_{L^{\infty}(\omega)}}$ | $\dfrac{\|u^{\varepsilon}-v_1^{\varepsilon}\|_{L^{\infty}(\omega)}}{\|u^{\varepsilon}\|_{L^{\infty}(\omega)}}$ | $\dfrac{\|\tilde{\theta}^{\varepsilon}-v_1^{\varepsilon}\|_{L^{\infty}(\omega)}}{\|u^{\varepsilon}\|_{L^{\infty}(\omega)}}$ | $\dfrac{\|(u^{\varepsilon}-\tilde{\theta}^{\varepsilon})'\|_{L^{\infty}(\omega)}}{\|(u^{\varepsilon})'\|_{L^{\infty}(\omega)}}$ | $\dfrac{\|(u^{\varepsilon}-v_1^{\varepsilon})'\|_{L^{\infty}(\omega)}}{\|(u^{\varepsilon})'\|_{L^{\infty}(\omega)}}$ | $\dfrac{\|\tilde{\theta}^{\varepsilon}-v_1^{\varepsilon})'\|_{L^{\infty}(\omega)}}{\|(u^{\varepsilon})'\|_{L^{\infty}(\omega)}}$ |
|---|---|---|---|---|---|---|
| 1/2 | 0.1772 | 0.1773 | 5.0662e-05 | 0.3689 | 0.3689 | 6.4858e-05 |
| 1/4 | 0.0392 | 0.0393 | 5.8285e-05 | 0.1797 | 0.1797 | 5.6607e-05 |
| 1/8 | 0.0105 | 0.0106 | 5.1947e-05 | 0.0551 | 0.0551 | 6.1300e-05 |
| 1/16 | 0.0030 | 0.0030 | 1.4789e-05 | 0.0291 | 0.0291 | 4.2297e-05 |
| 1/32 | 7.7461e-04 | 7.7794e-04 | 1.3399e-05 | 0.0147 | 0.0147 | 4.4260e-05 |
| 1/64 | 1.9444e-04 | 1.9717e-04 | 1.3230e-05 | 0.0072 | 0.0072 | 4.4636e-05 |
| 1/128 | 4.7256e-05 | 4.9425e-05 | 1.3135e-05 | 0.0036 | 0.0036 | 4.4877e-05 |
| 1/256 | 1.3556e-05 | 1.2365e-05 | 1.3117e-05 | 0.0018 | 0.0018 | 4.4942e-05 |

Table XII. Convergence of the error for $a_0 = 1/114$ (Example 5.1).

| $\varepsilon$ | $\dfrac{\|u^{\varepsilon}-\tilde{\theta}^{\varepsilon}\|_{L^2(\omega)}}{\|u^{\varepsilon}\|_{L^2(\omega)}}$ | $\dfrac{\|u^{\varepsilon}-v_1^{\varepsilon}\|_{L^2(\omega)}}{\|u^{\varepsilon}\|_{L^2(\omega)}}$ | $\dfrac{\|\tilde{\theta}^{\varepsilon}-v_1^{\varepsilon}\|_{L^2(\omega)}}{\|u^{\varepsilon}\|_{L^2(\omega)}}$ | $\dfrac{|u^{\varepsilon}-\tilde{\theta}^{\varepsilon}|_{H^1(\omega)}}{|u^{\varepsilon}|_{H^1(\omega)}}$ | $\dfrac{|u^{\varepsilon}-v_1^{\varepsilon}|_{H^1(\omega)}}{|u^{\varepsilon}|_{H^1(\omega)}}$ | $\dfrac{|\tilde{\theta}^{\varepsilon}-v_1^{\varepsilon}|_{H^1(\omega)}}{|u^{\varepsilon}|_{H^1(\omega)}}$ |
|---|---|---|---|---|---|---|
| 1/2 | 0.2198 | 0.2198 | 4.9235e-05 | 0.7441 | 0.7441 | 1.1564e-04 |
| 1/4 | 0.0498 | 0.0498 | 5.4289e-05 | 0.3943 | 0.3941 | 9.0161e-05 |
| 1/8 | 0.0098 | 0.0098 | 5.2807e-05 | 0.1437 | 0.1435 | 9.1670e-05 |
| 1/16 | 0.0022 | 0.0022 | 1.6372e-05 | 0.0478 | 0.0478 | 3.4093e-05 |
| 1/32 | 5.1461e-04 | 5.1791e-04 | 1.4632e-05 | 0.0166 | 0.0166 | 3.2820e-05 |
| 1/64 | 1.1998e-04 | 1.2212e-04 | 1.4447e-05 | 0.0068 | 0.0068 | 3.2840e-05 |
| 1/128 | 2.7089e-05 | 2.5045e-05 | 1.4298e-05 | 0.0031 | 0.0031 | 3.2752e-05 |
| 1/256 | 1.7007e-05 | 7.2070e-06 | 1.4264e-05 | 0.0016 | 0.0014 | 3.2889e-05 |

Table XIII. Convergence of the error for Example 5.2.

| $\varepsilon$ | $\dfrac{\|u^\varepsilon - \tilde{\theta}^\varepsilon\|_{L^\infty(\omega)}}{\|u^\varepsilon\|_{L^\infty(\omega)}}$ | $\dfrac{\|u^\varepsilon - v_1^\varepsilon\|_{L^\infty(\omega)}}{\|u^\varepsilon\|_{L^\infty(\omega)}}$ | $\dfrac{\|\tilde{\theta}^\varepsilon - v_1^\varepsilon\|_{L^\infty(\omega)}}{\|u^\varepsilon\|_{L^\infty(\omega)}}$ | $\dfrac{\|(u^\varepsilon - \tilde{\theta}^\varepsilon)'\|_{L^\infty(\omega)}}{\|(u^\varepsilon)'\|_{L^\infty(\omega)}}$ | $\dfrac{\|(u^\varepsilon - v_1^\varepsilon)'\|_{L^\infty(\omega)}}{\|(u^\varepsilon)'\|_{L^\infty(\omega)}}$ | $\dfrac{\|(\tilde{\theta}^\varepsilon - v_1^\varepsilon)'\|_{L^\infty(\omega)}}{\|(u^\varepsilon)'\|_{L^\infty(\omega)}}$ |
|---|---|---|---|---|---|---|
| 1/2 | 0.0201 | 0.0201 | 1.1319e-04 | 0.0943 | 0.0942 | 1.2343e-04 |
| 1/4 | 0.0081 | 0.0081 | 1.1432e-04 | 0.0504 | 0.0504 | 1.5476e-04 |
| 1/8 | 0.0027 | 0.0027 | 1.1485e-04 | 0.0274 | 0.0274 | 1.9519e-04 |
| 1/16 | 6.4478e-04 | 6.7477e-04 | 1.2202e-04 | 0.0139 | 0.0139 | 2.0149e-04 |
| 1/32 | 2.1540e-04 | 2.4465e-04 | 1.2224e-04 | 0.0070 | 0.0070 | 2.1863e-04 |
| 1/64 | 2.0915e-04 | 2.3819e-04 | 1.2231e-04 | 0.0035 | 0.0035 | 2.2713e-04 |

Table XIV. Convergence of the error for $a_0 = 10$ (Example 5.3).

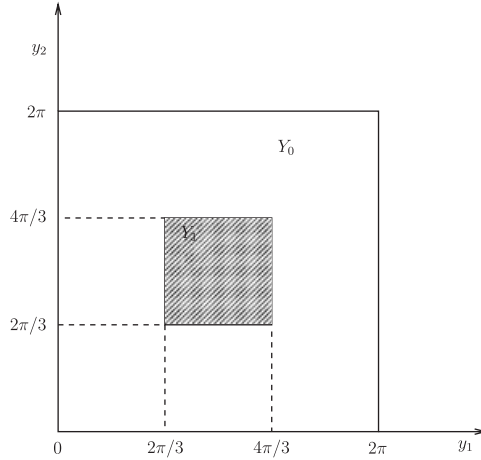| $\varepsilon$ | $\|u^\varepsilon - \theta^\varepsilon\|_{L^\infty(\cdot)}$ | $\|u^\varepsilon - v_2^\varepsilon\|_{L^\infty(\cdot)}$ | $\dfrac{\|u^\varepsilon - \theta^\varepsilon\|_{L^2(\cdot)}}{\|u^\varepsilon\|_{L^2(\cdot)}}$ | $\dfrac{\|u^\varepsilon - v_2^\varepsilon\|_{L^2(\cdot)}}{\|u^\varepsilon\|_{L^2(\cdot)}}$ | $\dfrac{\|u^\varepsilon - \theta^\varepsilon\|_{H^1(\cdot)}}{\|u^\varepsilon\|_{H^1(\cdot)}}$ | $\dfrac{\|u^\varepsilon - v_2^\varepsilon\|_{H^1(\cdot)}}{\|u^\varepsilon\|_{H^1(\cdot)}}$ |
|---|---|---|---|---|---|---|
| 1/2 | 0.0767 | 0.4548 | 0.0930 | 0.2302 | 0.2071 | 0.7279 |
| 1/4 | 0.0068 | 0.1196 | 0.0070 | 0.0627 | 0.0512 | 0.3518 |
| 1/8 | 0.0058 | 0.0344 | 0.0098 | 0.0199 | 0.0406 | 0.1547 |



Figure 6. Square representative cell $Y$.

Let us consider the representative cell as given in Figure 6 with

$$a_{k\ell 0} = \delta_{k\ell} \text{ (the Kronecker's symbol)} \quad \text{in } Y_0$$
$$a_{k\ell 1} = a_0 \delta_{k\ell} \quad \text{in } Y_1$$

where $a_{k\ell 0}$ and $a_{k\ell 1}$ represent the coefficients belonging to the regions $Y_0$ and $Y_1$, respectively.
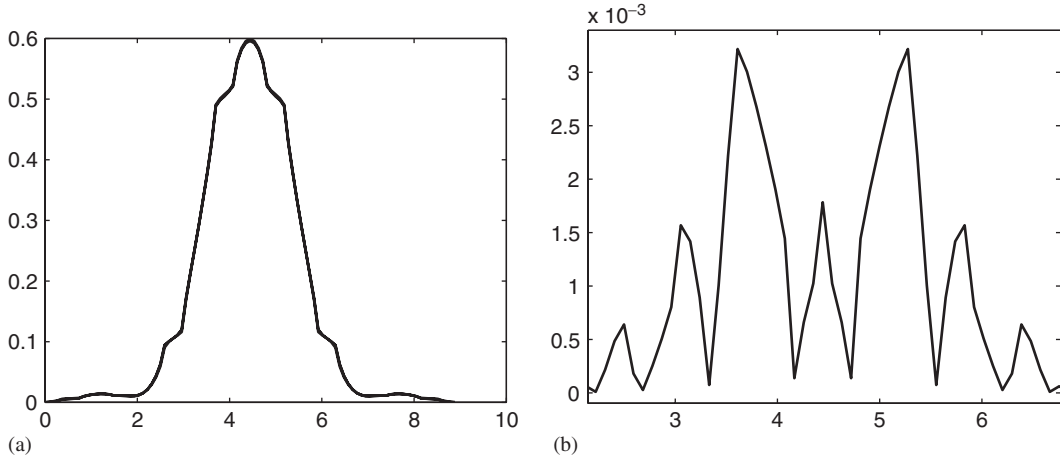
Figure 7. For $a_0 = 10$ and $\varepsilon = 1/4$: (a) $u^\varepsilon$; and (b) $|u^\varepsilon - \theta^\varepsilon|$.

*Example 5.3*
Consider the following boundary value problem. Let $u^\varepsilon$ be the solution of the following BVP:

$$A^\varepsilon u^\varepsilon + u^\varepsilon = f \quad \text{in } \Omega$$
$$u^\varepsilon = 0 \quad \text{on } \partial\Omega \tag{34}$$

where $A^\varepsilon$ is as defined in (3). In this example, we take $\Omega = \,]-2\pi, 2\pi[^2$, $f = (\sin x/x)(\sin y/y)$, $\varepsilon = 1/2, 1/4, 1/8$ and $a_0 = 10, 1/18, 1/144$ which arises from the physical problem of fibre-reinforced bars as studied by Bourgat and Lanchon [18].

Let us define the following functions and we may refer to them also as the classical first- and second-order correctors, respectively:

$$v_1^\varepsilon(x) = u^*(x) + \varepsilon\chi_k\left(\frac{x}{\varepsilon}\right)\frac{\partial u^*}{\partial x_k}(x)$$

and

$$v_2^\varepsilon(x) = v_1^\varepsilon(x) - \varepsilon^2\chi_{k\ell}\left(\frac{x}{\varepsilon}\right)\frac{\partial^2 u^*}{\partial x_k x_\ell}(x)$$

where $u^*$ is the homogenized solution, $\chi_k$ and $\chi_{k\ell}$ are, respectively, the solutions of the periodic cell problems (9) and (10). The determination of the first and second partial derivatives of $u^*$ in the above expressions have been explained in Reference [16].

Here also we have made a wide range of comparison between the Bloch approximation function $\theta^\varepsilon$, its Taylor approximation $\tilde{\theta}^\varepsilon$ with the exact solution $u^\varepsilon$, and the classical first- and second-order correctors $v_1^\varepsilon$, $v_2^\varepsilon$. In Figure 7(a), we plotted $u^\varepsilon$ along the diagonal $x = y$ of $\Omega$, respectively, in solid, broken, dotted lines. Figures 8(a) and 9(a) show $u^\varepsilon$, $\theta^\varepsilon$, $v_1^\varepsilon$, respectively, in solid, broken, dotted lines. Whereas, in Figure 9(b), we have presented $u^\varepsilon$, $\theta^\varepsilon$, $v_2^\varepsilon$, respectively,
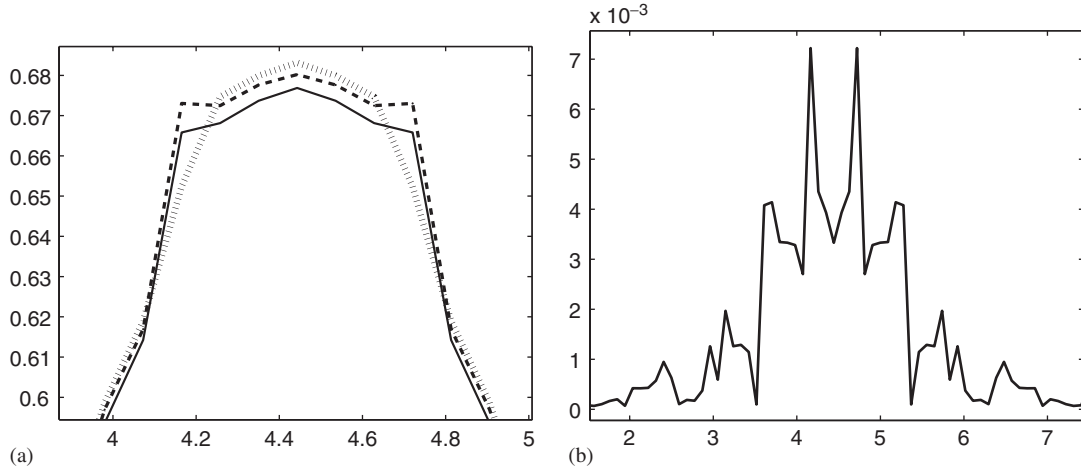
Figure 8. For $a_0 = 1/18$ and $\varepsilon = 1/8$: (a) $u^\varepsilon, \theta^\varepsilon, v_1^\varepsilon$; and (b) $|u^\varepsilon - \theta^\varepsilon|$.
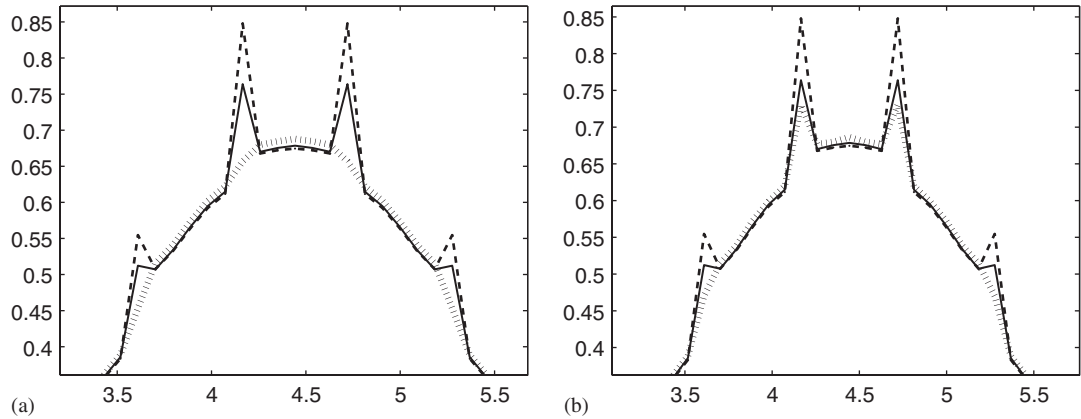


Figure 9. For $a_0 = 1/114$ and $\varepsilon = 1/8$: (a) $u^\varepsilon, \theta^\varepsilon, v_1^\varepsilon$; and (b) $u^\varepsilon, \theta^\varepsilon, v_2^\varepsilon$.

in solid, broken, dotted lines. As before, here also we have determined the errors in different norms in the subdomain $\omega = ] - \pi, \pi[^2$, and in the main peak (·) which depends on the parameter $\varepsilon$. These results are presented in Tables XIV–XIX and Figure 10.

From the above numerical experiments one can easily conclude the two facts mentioned earlier in the paper namely, that (i) the Bloch approximation function $\theta^\varepsilon$ produces better approximation for the exact solution $u^\varepsilon$ than the classical first- and second-order correctors $v_1^\varepsilon$, $v_2^\varepsilon$ at least in the smooth coefficient case, and provide a similar approximation as $v_1^\varepsilon$ and $v_2^\varepsilon$ in the discontinuous case, and (ii) the Taylor approximation function $\tilde{\theta}^\varepsilon$ performs in a very similar way as $v_1^\varepsilon$.

Table XV. Convergence of the error for $a_0 = 1/18$ (Example 5.3).

| $\varepsilon$ | $\|u^\varepsilon - \theta^\varepsilon\|_{L^\infty(\cdot)}$ | $\|u^\varepsilon - v_2^\varepsilon\|_{L^\infty(\cdot)}$ | $\|\theta^\varepsilon - v_2^\varepsilon\|_{L^\infty(\cdot)}$ | $\frac{\|u^\varepsilon - \theta^\varepsilon\|_{L^2(\cdot)}}{\|u^\varepsilon\|_{L^2(\cdot)}}$ | $\frac{\|u^\varepsilon - v_2^\varepsilon\|_{L^2(\cdot)}}{\|u^\varepsilon\|_{L^2(\cdot)}}$ | $\frac{\|\theta^\varepsilon - v_2^\varepsilon\|_{L^2(\cdot)}}{\|u^\varepsilon\|_{L^2(\cdot)}}$ |
|---|---|---|---|---|---|---|
| 1/2 | 0.0681 | 0.0405 | 0.1063 | 0.0949 | 0.0129 | 0.1039 |
| 1/4 | 0.0067 | 0.0121 | 0.0139 | 0.0060 | 0.0045 | 0.0094 |
| 1/8 | 0.0039 | 0.0077 | 0.0043 | 0.0050 | 0.0078 | 0.0044 |

Table XVI. Convergence of the error for $a_0 = 1/114$ (Example 5.3).

| $\varepsilon$ | $\|u^\varepsilon - \theta^\varepsilon\|_{L^\infty(\omega)}$ | $\|u^\varepsilon - v_2^\varepsilon\|_{L^\infty(\omega)}$ | $\|\theta^\varepsilon - v_2^\varepsilon\|_{L^\infty(\omega)}$ | $\frac{\|u^\varepsilon - \theta^\varepsilon\|_{L^2(\omega)}}{\|u^\varepsilon\|_{L^2(\omega)}}$ | $\frac{\|u^\varepsilon - v_2^\varepsilon\|_{L^2(\omega)}}{\|u^\varepsilon\|_{L^2(\omega)}}$ | $\frac{\|\theta^\varepsilon - v_2^\varepsilon\|_{L^2(\omega)}}{\|u^\varepsilon\|_{L^2(\omega)}}$ |
|---|---|---|---|---|---|---|
| 1/2 | 1.0128 | 0.8550 | 1.3202 | 0.7089 | 0.3222 | 0.6666 |
| 1/4 | 0.8279 | 0.1775 | 0.8211 | 0.2345 | 0.0666 | 0.2343 |
| 1/8 | 0.0839 | 0.0523 | 0.1172 | 0.0342 | 0.0151 | 0.0414 |

Table XVII. Convergence of the error for $a_0 = 10$ (Example 5.3).

| $\varepsilon$ | $\|u^\varepsilon - \tilde{\theta}^\varepsilon\|_{L^\infty(\omega)}$ | $\|u^\varepsilon - v_1^\varepsilon\|_{L^\infty(\omega)}$ | $\|\tilde{\theta}^\varepsilon - v_1^\varepsilon\|_{L^\infty(\omega)}$ | $\frac{\|u^\varepsilon - \tilde{\theta}^\varepsilon\|_{L^2(\omega)}}{\|u^\varepsilon\|_{L^2(\omega)}}$ | $\frac{\|u^\varepsilon - v_1^\varepsilon\|_{L^2(\omega)}}{\|u^\varepsilon\|_{L^2(\omega)}}$ | $\frac{\|\tilde{\theta}^\varepsilon - v_1^\varepsilon\|_{L^2(\omega)}}{\|u^\varepsilon\|_{L^2(\omega)}}$ |
|---|---|---|---|---|---|---|
| 1/2 | 0.0200 | 0.0234 | 0.0433 | 0.0269 | 0.0266 | 0.0046 |
| 1/4 | 0.0072 | 0.0318 | 0.0346 | 0.0099 | 0.0117 | 0.0053 |
| 1/8 | 0.0055 | 0.0117 | 0.0091 | 0.0070 | 0.0076 | 9.3842e-04 |

Table XVIII. Convergence of the error for $a_0 = 1/18$ (Example 5.3).

| $\varepsilon$ | $\frac{\|u^\varepsilon - \tilde{\theta}^\varepsilon\|_{L^2(\omega)}}{\|u^\varepsilon\|_{L^2(\omega)}}$ | $\frac{\|u^\varepsilon - v_1^\varepsilon\|_{L^2(\omega)}}{\|u^\varepsilon\|_{L^2(\omega)}}$ | $\frac{\|\tilde{\theta}^\varepsilon - v_1^\varepsilon\|_{L^2(\omega)}}{\|u^\varepsilon\|_{L^2(\omega)}}$ | $\frac{\|u^\varepsilon - \tilde{\theta}^\varepsilon\|_{H^1(\omega)}}{\|u^\varepsilon\|_{H^1(\omega)}}$ | $\frac{\|u^\varepsilon - v_1^\varepsilon\|_{H^1(\omega)}}{\|u^\varepsilon\|_{H^1(\omega)}}$ | $\frac{\|\tilde{\theta}^\varepsilon - v_1^\varepsilon\|_{H^1(\omega)}}{\|u^\varepsilon\|_{H^1(\omega)}}$ |
|---|---|---|---|---|---|---|
| 1/2 | 0.0451 | 0.0454 | 0.0032 | 0.1060 | 0.1058 | 0.0251 |
| 1/4 | 0.0161 | 0.0168 | 0.0037 | 0.0827 | 0.0834 | 0.0281 |
| 1/8 | 0.0081 | 0.0084 | 8.6196e-04 | 0.0404 | 0.0402 | 0.0113 |

Table XIX. Convergence of the error for $a_0 = 1/114$ (Example 5.3).

| $\varepsilon$ | $\frac{\|u^\varepsilon - \tilde{\theta}^\varepsilon\|_{L^2(\omega)}}{\|u^\varepsilon\|_{L^2(\omega)}}$ | $\frac{\|u^\varepsilon - v_1^\varepsilon\|_{L^2(\omega)}}{\|u^\varepsilon\|_{L^2(\omega)}}$ | $\frac{\|\tilde{\theta}^\varepsilon - v_1^\varepsilon\|_{L^2(\omega)}}{\|u^\varepsilon\|_{L^2(\omega)}}$ | $\frac{\|u^\varepsilon - \tilde{\theta}^\varepsilon\|_{H^1(\omega)}}{\|u^\varepsilon\|_{H^1(\omega)}}$ | $\frac{\|u^\varepsilon - v_1^\varepsilon\|_{H^1(\omega)}}{\|u^\varepsilon\|_{H^1(\omega)}}$ | $\frac{\|\tilde{\theta}^\varepsilon - v_1^\varepsilon\|_{H^1(\omega)}}{\|u^\varepsilon\|_{H^1(\omega)}}$ |
|---|---|---|---|---|---|---|
| 1/2 | 0.0737 | 0.0739 | 0.0034 | 0.2142 | 0.2143 | 0.0262 |
| 1/4 | 0.0471 | 0.0474 | 0.0040 | 0.3389 | 0.3384 | 0.0283 |
| 1/8 | 0.0204 | 0.0207 | 9.1488e-04 | 0.2549 | 0.2532 | 0.0119 |

## 6. CONCLUSION

A numerical method based on the Bloch approximation is presented here for the numerical solution of elliptic PDEs with rapidly oscillating periodic coefficients. The numerical solution
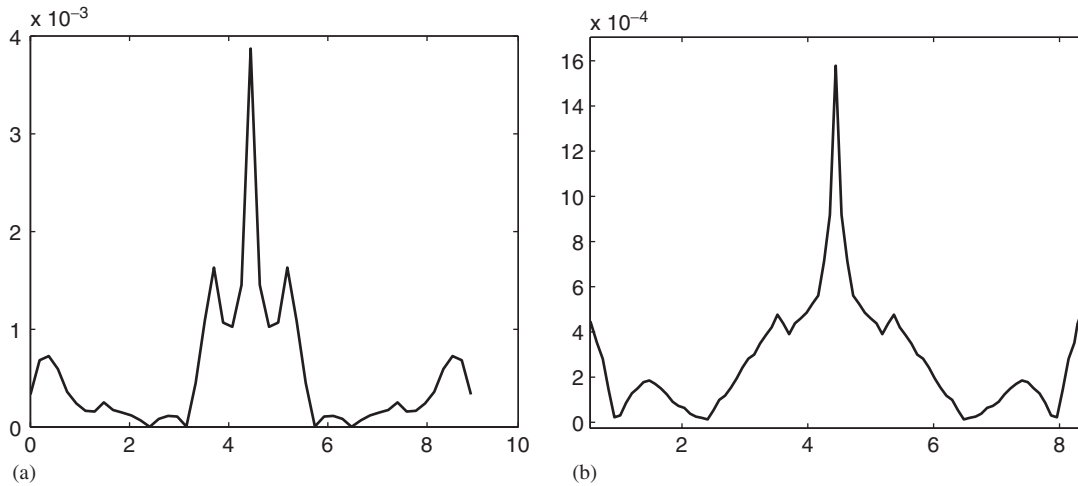
Figure 10. Plots of $|u^\varepsilon - \tilde{\theta}^\varepsilon|$ inside $\omega = ] - \pi, \pi[^2$: (a) For $a_0 = 10$ and $\varepsilon = 1/2$; and (b) for $a_0 = 1/114$ and $\varepsilon = 1/8$.

of such problems is difficult to compute by direct methods because of the presence of rapidly oscillating coefficients. In order to capture the local oscillations in $u^\varepsilon$ one has to use a very small step size, and an approximation method for $u^\varepsilon$ is required. Apart from the classical homogenization process (which includes the first- and second-order corrector terms), we have introduced here the Bloch approximation $\theta^\varepsilon$. As it was mentioned in the abstract that $\theta^\varepsilon$ provides better approximations to $u^\varepsilon$ than the classical first- and second-order corrector terms, specifically in the case of high-contrast materials. Comparing the results given in Tables IV and VII we conclude that there is quite a bit of gain in $H^1$ semi-norm in contrast to $L^2$ and $L^\infty$ norms in the case of high-contrast materials, i.e. with spectral approach one avoids spurious oscillations that appear if one uses classical correctors. Theoretical proof of this phenomena is lacking in the literature. Moreover, one can use the Taylor approximation $\tilde{\theta}^\varepsilon$ of $\theta^\varepsilon$ as given in (30) which does not require more computation except the auxiliary functions $\chi_k$ (which can be determined either by (15) or by solving (9) directly) and provides almost the same approximation as the first-order corrector term. As a result, we can conclude that $\theta^\varepsilon$ is a powerful alternative tool for the numerical solution of such problems.

As mentioned in the introduction, our numerical results describe the interior oscillations of the solution on a relatively compact open subsets $\omega \subset\subset \Omega$. It would be interesting to see how the size of the domain $\omega$ affects the convergence rate presented in the tables. Further, it could be interesting to extend the present analysis to the case of locally periodic media, and even for random media.

## REFERENCES

1. Sánchez-Palencia E. *Non-homogeneous Media and Vibration Theory*. Lecture Notes in Physics, vol. 127. Springer: Berlin, 1980.
2. Allaire G, Conca C, Vanninathan M. Spectral asymptotics of the Helmholtz model in fluid-solid structures. *International Journal for Numerical Methods in Engineering* 1999; **46**:1463–1504.
3. Conca C, Planchard J, Vanninathan M. *Fluids and Periodic Structures*. Research in Applied Mathematics, vol. 38. Wiley/Masson: New York/Paris, 1995.
4. Bensoussan A, Lions J-L, Papanicolaou G. *Asymptotic Analysis for Periodic Structures*. North-Holland: Amsterdam, 1978.
5. Conca C, Vanninathan M. Homogenization of periodic structures via Bloch decomposition. *SIAM Journal on Applied Mathematics* 1997; **57**:1639–1659.
6. Conca C, Orive R, Vanninathan M. Bloch approximation in homogenization and applications. *SIAM Journal on Mathematical Analysis* 2002; **33**:1166–1198.
7. Allaire G, Conca C. Boundary layers in the homogenization of a spectral problem in fluid-solid structures. *SIAM Journal on Mathematical Analysis* 1997; **29**:343–379.
8. Avellaneda M, Hou T, Papanicolaou G. Finite difference approximations for partial differential equations with rapidly oscillating coefficients. *Mathematical Modelling and Numerical Analysis* 1991; **25**:693–710.
9. Orive R, Zuazua E. Finite difference approximation of homogenization problems for elliptic equations. *Multiscale Modeling and Simulation* 2005; **4**:36–87.
10. Hou TY, Wu XH. A multiscale finite element method for elliptic problems in composite materials and porous media. *Journal of Computational Physics* 1997; **134**:169–189.
11. Avellaneda M, Berlyand L, Clouet J-F. Frequency-dependent acoustics of composites with interfaces. *SIAM Journal on Applied Mathematics* 2000; **60**:2143–2181.
12. Bernardi C, Maday Y. *Approximations Spectrales de problèmes aux limites elliptiques*. Collection Mathématiques and Applications, vol. 10. Springer: Paris, 1993.
13. Gottlieb D, Orzag S. *Numerical Analysis of Spectral Methods*, *Theory and Applications*. SIAM Publications: Philadelphia, 1977.
14. Sivaji Ganesh S, Vanninathan M. Bloch wave homogenization of scalar elliptic operators. *Asymptotic Analysis* 2004; **39**:15–44.
15. Bloch F. Über die quantenmechanik der electronen in kristallgittern. *Zeitschrift Fur Physik* 1928; **52**: 555–600.
16. Conca C, Natesan S. Numerical methods for elliptic partial differential equations with rapidly oscillating coefficients. *Computer Methods in Applied Mechanics and Engineering* 2003; **192**:47–76.
17. Bourgat J. Numerical experiments of the homogenization method for operators with periodic coefficients. *Technical Report 277*, Institut de Recherche d'Informatique et d'Automatique, Le Chesnay, France, 1978.
18. Bourgat J, Lanchon H. Application of the homogenization method to composite materials with periodic structures. *Technical Report 208*, Institut de Recherche d'Informatique et d'Automatique, Le Chesnay, France, 1976.